MATERIALS IN EXTREME ENVIRONMENTS FOR ENERGY, ACCELERATORS AND SPACE APPLICATIONS AT ELI-NP

T. ASAVEI[1,*], M. TOMUT[2], M. BOBEICA[1], S. AOGAKI[1], M.O. CERNAIANU[1], M. GANCIU[3], S. KAR[4], G. MANDA[5], N. MOCANU[6], L. NEAGU[1], C. POSTOLACHE[6], D. SAVU[6], D. STUTMAN[1], D. VIZMAN[7], D. URSESCU[1], S. GALES[1], N. V. ZAMFIR[1]

[1]ELI-NP, "Horia Hulubei" National Institute for Physics and Nuclear Engineering, 30 Reactorului Street, RO-077125, Bucharest-Magurele, Romania

[2]GSI Helmholzzentrum für Schwerionenforschung GmbH, 64291 Darmstadt, Germany

[3]National Institute for Laser, Plasma and Radiation Physics, 409 Atomistilor Street, RO-077125, Bucharest-Magurele, Romania

[4]School of Mathematics and Physics, The Queen's University of Belfast, BT7 1NN Belfast, UK

[5]Cellular and Molecular Medicine Department, "Victor Babes" National Institute of Pathology, 99-101 Splaiul Independentei, Bucharest 050096, Romania

[6]"Horia Hulubei" National Institute for Physics and Nuclear Engineering, 30 Reactorului Street, RO-077125, Bucharest-Magurele, Romania

[7]Faculty of Physics, West University of Timisoara, Bd. V. Parvan 4, 300223 Timisoara, Romania

*Corresponding author *Email:* theodor.asavei@eli-np.ro

Abstract. As a leading facility in laser-driven nuclear physics, ELI-NP will develop innovative research in the fields of materials behavior in extreme environments and radiobiology, with applications in the development of accelerator components, new materials for next generation fusion and fission reactors, shielding solutions for equipment and human crew in long term space missions and new biomedical technologies. The specific properties of the laser-driven radiation produced with two lasers of 1 PW at a pulse repetition rate of 1 Hz each are an ultra-short time scale, a relatively broadband spectrum and the possibility to provide simultaneously several types of radiation. Complex, cosmic-like radiation will be produced in a ground-based laboratory allowing comprehensive investigations of their effects on materials and biological systems. The expected maximum energy and intensity of the radiation beams are 19 MeV with 10^9 photon/pulse for photon radiation, 2 GeV with 10^8 electron/pulse for electron beams, 60 MeV with 10^{12} proton/pulse for proton and ion beams and 60 MeV with 10^7 neutron/pulse for a neutron source. Research efforts will be directed also towards measurements for radioprotection of the prompt and activated dose, as a function of laser and target characteristics and to the development and testing of various dosimetric methods and equipment.

Key words: ELI-NP, material science, space science

1. INTRODUCTION

Dosimetry, ionizing radiation metrology and radiation induced biological damage are major active research areas in nuclear (bio)physics and engineering. Their applications extend from the nuclear power plants to medicine and from space science to material science and to accelerators engineering. Typical research that will be described in this paper relates to testing of materials for accelerator sub-systems, testing of materials for space science (electronics components), material science research (surface and volume modification, nanotechnology), biomedical research (radiation effects on cells, tissues, organisms), testing and development of detectors as well as testing of irradiated optical components.

2. PHYSICS CASES

2.1 TESTING OF NEW MATERIALS FOR ACCELERATOR COMPONENTS

In the framework of this technical design report (TDR) the study of materials behaviour in extreme environments will be a central topic, with a direct application to the development of accelerator components and societal applications like the understanding of structural materials degradation in next generation fusion and fission reactors or the shielding of equipment and human missions in outer space. Testing of novel materials for accelerator components at the future high–power facilities like the Facility for Antiproton and Ion Research (FAIR), the High Luminosity Large Hadron Collider (HL-LHC), the Facility for Rare Isotope Beams (FRIB), neutrino factories and the European Spallation Source (ESS) in conditions of radiation, temperature and pressure similar to the operation scenarios would be possible by using "cocktails" of laser driven particles and laser induced shock waves. The Extreme Light Infrastructure-Nuclear Physics (ELI-NP) through the experimental area E5 offers a unique testing facility complementary to accelerator irradiation. The availability of two high-intensity short-pulse lasers would enable pump-probe experiments using laser based diagnostic enabling structural degradation studies during irradiation on a much finer time scale.

2.1.1. Testing of accelerator materials at fast energy deposition and mixed radiation fields

With the development of new high-power accelerator facilities, materials that have been traditionally used for targets, beam protection elements, beam tube and

windows are facing new challenges, being solicited to their limits by extreme thermo-mechanical loads and radiation fields during operation. Particularly in the case of accelerators using bunched beams like FAIR, the Large Hadron Collider (LHC) and neutrino production facilities, targets and selected accelerator components will experience shock waves induced by energy deposited within the beam spot. Experiments under similar operation conditions are required to develop and apply high speed monitoring techniques, and to supply more detailed information for better understanding the failure mechanism by crack formation, propagation, and fracture processes. Experimental results will allow lifetime estimates for these elements and additionally provide input data for simulations.

A. Super-FRS target at FAIR

At the future FAIR facility, to be built at GSI Darmstadt, it will be possible to perform experiments in different fields of physics in a parameter range that is presently inaccessible. A wide range of particles with energies up to 1.5 A GeV will be used for the production of fragments by projectile fragmentation/fission at the proposed superconducting fragment separator (Super-FRS) [1]. The Super-FRS will be the most powerful in-flight separator for exotic nuclei at relativistic energies. Rare isotopes of all elements up to uranium will be produced and spatially separated within some hundred nanoseconds, enabling the study of very short-lived nuclei.

As the resolving power of the Super-FRS is inversely proportional to the beam spot radius, it is required to minimize the transversal beam dimensions at the position of the production target. The final goal would be a primary driver beam radius in x and y direction of the order of 1-2 mm. The combination of high intensities of a driver beam, large projectile Z-values, and small radii of the driver-beam spot will lead to high induced power densities inside the targets. Similar to the present fragment separator facility, both slow and fast extraction from the SIS100 heavy ion synchrotron at FAIR will be used: the former with typical extraction times of a few seconds for counter experiments at the experimental caves, the latter for experiments with radioactive secondary beams in the storage rings where driver beams with a typical pulse length of 50 ns are required.

The high instantaneous power-deposition in the target by fast-extracted beams (up to 200 GW) may lead to explosive regimes [2]. As a result, the target could be destroyed by a single beam pulse. Therefore, new technical developments for the production targets are required in order to profit from the full potential of the Super-FRS for exotic nuclei production. Furthermore, the high intensities of a driver beam will change the technical requirements for the beam dump. A proper technical solution to the problems connected with the specific energy deposition of heavy ions in the fast and the slow extraction modes has to be found.

In slow extraction mode, the expected maximum deposited beam power of 12 kW induced by ^{238}U driver beam is comparable to the values found in operating

facilities (*e.g.*, at the Paul Scherrer Institute (PSI) [3]). Following the longstanding experience at PSI, a concept of rotating graphite wheel as a Super-FRS target has been chosen [4]. On the other hand, in fast extraction mode, two options were initially considered namely, the same rotating-wheel concept which is also chosen for fast extraction with a low deposited specific beam power (low projectile Z and/or low intensities, extended size of the beam spot) and, for the highest power densities a windowless liquid-metal has been initially considered, but simulation have shown that the jet will be destroyed by the pulsed beam.

The concept of a rotating-wheel target should be applied for fast-extracted beams, as long as the critical parameters of graphite (*e.g.,* temperature, pressure) are not exceeded. For this purpose, a detailed knowledge on the response of graphite material induced by pulsed high-intensity ion beams is essential. The steep temperature gradients generated in solid materials during a passage of beam particles excite stress waves. These stress waves propagate then in different directions towards the surface of the solid target, where they are rejected and excite natural oscillations of the target. After a few reflections the stress waves vanish due to damping.

Experiments on graphite target response under pulsed ion beams have been done up to now at the high energy, high temperature (HHT) beamline at the GSI Helmholtz Center for Heavy Ion Research with fast extracted relativistic ion beams and at the Universal Linear Accelerator (UNILAC) based also at GSI with GeV U ions pulses 100 µs long. In both type of experiments, the beam intensity was not high enough to lead to thermo-mechanical failure of the pristine target. Failure in the last situation was due to decreased fatigue resistance of target material that has been accumulating radiation damage (Fig. 1). The energy deposition/pulse can be increased by using very intense proton and ion beams produced by laser acceleration or directly by exposing the material to laser beam.

Fig. 1 – Failure of graphite target foils exposed to 5×10^{14} ^{238}U ions/cm^2, 150 µs pulse length, 0.4 Hz, 4.8 MeV/u

B. Secondary collimators for HL-LHC

Particle beam propagation is associated with unavoidable losses. The losses include: primary halo of protons – managed by primary collimator, secondary halo – managed by secondary collimator and tertiary halo managed by absorber.

At each stage there are electron and hadron showers accompanying proton halos. Behind the collimators there are SC magnets and particle physics experiments. In some solutions, like in SIS 100 at FAIR, the primary collimator is a thin foil which acts like a scatterer of the halo particles and the secondary collimators in a form of bulky blocks are necessary to absorb the scattered particles. Crystals (acting as primary aperture) assisted collimation assumes usage of elastic and diffractive scattering. The crystal is bent and behaves like a Bragg grating for scattered particles.

The collimation system must satisfy two main functions: Multi-stage Beam Cleaning (BC), *i.e.* removing stray particles which would induce quenches in SC magnets; and Machine Protection, *i.e.* shielding the other machine components from the catastrophic consequences of beam orbit errors. Classical C-C carbon composite collimators are affected by intrinsic limitations which may ultimately limit LHC performances: low Z-material of the collimator limits cleaning efficiency, poor electrical conductivity material of collimator means high RF impedance, limited radiation hardness of collimator material means reduced lifetime.

Innovative materials are needed for accelerator collimator jaws for the upgrade of the LHC. The research on collimator and materials for higher beam power (ColMat) consists of research and development of novel materials, advanced numerical simulations, material testing, prototype design and manufacturing. ColMat research and development within the European Coordination for Accelerator Research and Development (EuCARD) project focuses on Metal Matrix Composites (MMC) with diamond and graphite reinforcement as they have the potential to combine the properties of diamond and graphite (high thermal conductivity, low density, low CTE) with those of metals (strength, high Poisson ratio, high Young's modulus). Sintering techniques include rapid hot pressing (RHP) and liquid infiltration. Spark plasma sintering (SPS) is a technology of the future. Materials under investigation are Copper-diamond (Cu-CD) and Molybdenum- Graphite (Mo-Gr). The materials are tested for: shock wave analysis, smooth particle hydrodynamics (material fragmentation), irradiation studies with proton and carbon ion beams – swelling measurements and mechanical tests.

Cu-CD composites are produced by RHP from 60% diamond and 40% Cu. No diamond degradation in reducing atmosphere is observed. Diamond graphitization starts at approximately 1300° C. Thermal conductivity is around 500 W/mK, and electrical conductivity 12.6 MS/m. There is no direct interface between Cu and CD because of a lack of affinity. Mechanical strength is average 120 MPa. Cu low melting point limits applications for highly energetic accidents.

Mo-Gr composites are under intense research and development. Graphite

addition has low CTE, low density, high thermal conductivity, high melting point and high shock wave damping. The properties are similar to Mo-CD but the mechanical strength is not yet satisfactory. One of the solutions is to use Mo-Gr/Mo sandwich which consists of Mo-Gr core with Mo layers.

The aims of collimator material experiments at ELI-NP are: to test traditional and novel materials under extreme conditions they may encounter in case of accidental beam impacts; to quantify material damage for LHC operating scenarios; to fully characterize novel materials currently under development for new generation of collimators; to benchmark advanced numerical solutions, in-depth but based on limited and scarce published data on material constitutive models; to collect, mostly in real time, experimental data on constitutive models of materials, including equation of state, strength models, failure models.

There are several main objectives for material research and development for accelerator technology. These objectives have been turned into a set of figures of merit (FoM) to assess relevant materials. For instance, in order to reduce the RF impedance of the material one needs to maximize its electrical conductivity, to maintain/improve geometrical stability in nominal conditions one needs to maximize the stability indicator Steady-state Stability Normalized Index (SSNI), to maintain the robustness in accidental scenarios one needs to maximize the robustness indicator Transient Thermal Shock Normalized Index (TSNI), to improve cleaning efficiency by relevant absorption rate one needs to increase radiation and nuclear interaction length by high enough atomic number, to improve the maximum operational temperature one needs to increase the melting temperature. Additional standard requirements include radiation hardness, ultra-high vacuum (UHV) compatibility and so forth.

C. Experiments

We propose to perform the experiment with exposure of thin targets, as primary or secondary target, to increasing intensities of laser, or laser-generated proton, electron and ion beams.

For in-situ monitoring and alignment of our graphite foil targets, cameras will be used. The vibration amplitudes and velocities of the sample surface and spalled fragments will be measured by means of a VISAR and streak cameras placed outside the target chamber. Mirrors will be used for alignment on the targets. The survival to increasing energy density, of materials foreseen as candidates for accelerator components will be investigated by varying the intensity of laser accelerated particle beams. This will be achieved either by changing the intensity of the laser pulse or by changing the distance between the target for laser acceleration and our secondary target.

Off-line tests of exposed samples will include structural investigations using profilometry XRD, electron microscopy, Raman spectroscopy and mechanical tests

using nanoindentation. These experimental techniques will help in understanding what is the failure mechanism of targets for high intensity pulsed beams and determine failure criteria for these targets. Post-irradiation microstructural investigations and positron annihilation will provide insight into the physics of defect evolution and recombination at short time scale in target materials. Advanced multi-scale materials simulations can be used in conjunction with these experiments to develop models of the physical phenomena governing the response of materials under extreme environments.

2.1.2. Laser induced shock waves

By focusing a short-pulsed laser (ns to fs pulses) on the surface of a solid target, reaction shock waves can be induced provided that the power density of the focused beam is high enough (larger than 10^9 W/cm^2). The laser induced shock waves are of great importance for studies of matter in extreme conditions, as they permit investigations of high-temperature high-pressure regimes in solids. The pressure obtained in the case of shock wave compression is of the order of magnitude of hundreds of GPa.

A laser pulse creates a spherical shock wave in the target material. Overlapping of multiple shock waves is also possible by generating spatially separated pulses and thus shock waves interference can be achieved [5].

2.1.3. On-line laser based diagnostic

Testing novel composite materials and proposed beam protection elements and target designs will aim at increasing the performance at nominal beam intensities. Online imaging techniques based on PW laser-generated X-rays, protons, and neutrons are new means for acquiring time-resolved information of transient phenomena involved in ion-beam induced shock propagation. For lifetime estimation of the Super-FRS target and beam catchers at FAIR and collimators at LHC, shock and stress waves experiments will be performed on samples that already accumulated radiation damage in-situ and which cannot be transported outside irradiation facilities for experiments due to radiation safety concerns. Detecting the generation of such extreme conditions in dense samples and actually measuring its properties will require advanced diagnostic capabilities based on highly penetrating probe radiation. In addition, extreme brightness is necessary to provide sufficient flux within the short life-time of the samples at extreme conditions. High-energy high-intensity laser systems allow generation of a variety of highly penetrating secondary radiation at ultra-high intensities.

2.1.4. Pump-probe experiments on radiation-induced defect cluster evolution and ion track formation processes in solids

Time-resolved in-situ analysis will permit us to explore ultra-short processes associated with the formation of ion tracks in solids using ultrafast laser-based diagnostic. At present, the coupling of the densely excited electron subsystem to the motion of the atoms in the lattice is neither understood nor experimentally accessible. Electronic excitation processes and subsequent lattice heating and relaxation occur on a time scale spanning from hundreds of femtoseconds to tens of picoseconds. Access to experimental data in this short time window will allow benchmarking of existing track models at ambient or high-pressure. Besides the track formation process, it is also important to monitor in-situ the dynamics of irradiation induced defects on larger time scales. Clustering, defect-sinks annihilation and temperature-induced annealing are all important processes that determine dimensional changes, thermo-mechanical and electrical properties of irradiated materials with large impact on their nuclear application. A very dynamic field of using laser-generated particles and radiation such as X-rays, positrons, protons and neutrons as probes for investigating these processes in pump-probe experiments is now spreading in different scientific communities from hard condensed matter to high-energy density matter.

2.1.5. Laser modification of materials for accelerator applications

Femtosecond lasers can be used for materials micromachining and local generation of non-equilibrium phases. 3D architectures can be generated using both beams. One example would be "writing" of complex graphitized electrode structures in diamond detectors for increased radiation hardness.

2.2 TESTING AND DEVELOPMENT OF DETECTORS

Building of the new ELI-NP facility should comply with Romanian Radiation Safety Norms developed by Romanian Regulatory Body – National Commission for Nuclear Activity Control (CNCAN). In this way the licensing of ELI-NP will be performed in steps. First step is Construction License. Construction License allows to mount the accelerator and high intensity laser source. Also the construction license allows checking the radiation protection shielding. Radiation protection shielding refers to walls, doors, ceilings and so forth. Radiation protection measurements should be given priority during all mounting steps: for accelerator mounting, for high intensity PW laser and at the end for both accelerator and laser. There are needs to measure the primary electron beam and gamma beams. Due to high energy gamma beams (19.5 MeV) we expect to have photo-neutron contamination too. From these

reasons the radiation protection of workers is very important and should comply with Radiation Safety Norms.

Radiation protection measurement performed in order to check the radiation protection shielding will address the worst operating conditions: highest energy and highest intensity of the electron and gamma beams. Measurements will be performed for: primary beam (electron or gamma beam), measurement in controlled area (irradiation room and control room), and in the survey area (area close to control area). Radiation protection measurements in primary beam will be performed using ionization chambers like STARDOOR. These chambers are calibrated to primary standard at PTB which provide higher measurement precision. The ISO 17025:2005 accreditation provides high quality in delivered measurement results according to applicable standards.

The field characteristics can be tested using a film densitometry method. A special film is exposed to electron or gamma beam, and then is read using a high precision analogical densitometer. 3D reconstruction in film densitometry provides information regarding radiation field characteristics, *e.g.* beam distribution, field homogeneity, penumbra etc., as well as amount of exposure.

The measurement in controlled area involves measurements of all leakage photons, direct beam photons, scattered photons, electrons and neutrons. Because there is a combined exposure field, the radiation protection measurements will be performed to obtain isodose area distribution. These measurements will provide information on hot point of exposure. The measurement will be performed with high precision spherical ionization chamber. The photoneutrons will be measured with Kuhn ionization chamber. All measurements will be doubled with film dosimetry method.

The investigations in control room and all survey area will provide information on exposure level of professional exposure occupational personnel and for public exposure. The measurement for radiation protection of workers and public should be performed with ionization chamber. The STARDOOR laboratory will perform measurements with spherical chamber. All measurements will be doubled with film dosimetry method. The exposure to ionizing radiation in control room and in survey area should comply with CNCAN requirements.

New research will be performed by STARDOOR laboratory in development of new radiation detection systems for example continuing the work on new radiation detection development based on optical fiber. The previous laboratory's work shows a possibility to use optical fiber as real time dosimeter.

We would like to investigate also the possibility to use SSNTD type CR39 as neutron detectors. Shape of neutron track in CR39 detector could provide information on neutron energy. STARDOOR laboratory also will study the thin film reaction to electron and photon beam.

2.3 EVALUATION OF HIGH ENERGY IONIZING RADIATION EFFECTS IN MATERIALS

2.3.1. High energy ionizing radiation in space environment

Space vehicles, satellites, equipment and astronauts must perform current activities in a hostile environment under stress agents such as: natural space radiation, exposure at cryogenic or high temperature conditions, high vacuum environment and high velocity cosmic dust and micrometeorites.

A. Space radiation environments

Cosmic rays (CR), discovered in 1912 by Victor Hess, are high energy particles generated by astrophysical phenomena [6]. The CR can be classified in two main classes: (a) transient radiation and (b) trapped radiation.

A.1 The transient radiation

The transient CR consists of Galactic Cosmic Ray (GCR) and Solar Cosmic Radiation (SCR). GCR generated in Milky Way space and outside of the galaxy, contain mainly hadrons components (about 85% protons, 12% helium nuclei, and less than 1% heavy ions with composition [7], almost 2% leptons [8] and electromagnetic particles (gamma and X-rays). Maximum energy of the particles is more than $1.6 \cdot 10^{-17}$ J (1 TeV).

SCR is composed of two categories of radiation, low energy solar-wind particles that are constantly emitted from the sun, and highly energetic Solar Particle Events (SPEs). Solar wind is a neutral, continuous stream of charged particles emanating from Sun's corona. Solar wind consists of protons (95% relative abundance), helium nuclei (approximately 4% relative abundance), other heavy ions (less than 1% relative abundance) and electrons. The solar wind particles energies are lower than a few keVs.

SPEs are high energy and high density particles generated by two solar storm phenomena, (a) solar flares, and (b) coronal mass ejections (CMEs). Solar flares are large explosive events associated with intense releases of energy (electromagnetic rays) and accelerated particles, (especially protons and electrons). Energy of the charges particles and gamma rays can reach values of the $1.6 \cdot 10^{-10}$ J (1 GeV). CMEs are material ejections from Sun's photosphere into the interplanetary space. A large CME can eject approximately 10^{17} grams of plasma into solar system space in several hours. The frequency of CME is correlated with the Sun and sunspots cycles [9].

The typical 11 year cycle of the sun is characterized by a period of four years of relative inactivity, followed by seven years with increased numbers of SPE's. These ejections of high energy particles are highly directed, affecting only small regions of space, but are characterized by very high particle fluxes and can be extremely hazardous to space systems and crewed space vehicles and astronauts. During the period of minimum solar activity, about one CME per week has been determined; during maximum solar activity, two to three CME per day were observed [9]. The energy is usually up to order of $1.6 \cdot 10^{-9}$ J (100 MeV), but exceptionally can reach approximately $1.6 \cdot 10^{-11}$ J (10 GeV). The flux is strongly related to the solar cycle, varying therefore also by several orders of magnitude [10, 11].

A.2. Trapped radiations

The trapped radiations represent energetic charged particles long time retained by the magnetic traps of the planetary magnetic fields. For the Earth, the interaction between solar wind and GCR with terrestrial magnetic field results in two distinct torus-shaped layers around the Earth, named Van Allen belts. In the inner belt consists of trapped protons with energies between $6.4 \cdot 10^{-12}$ J (40 keV) and $0.8 \cdot 10^{-10}$ J (500 MeV) [12]. The outer belt consist mainly of trapped electrons with energies in $6.4 \cdot 10^{-12}$ J (40 keV) and $1.12 \cdot 10^{-9}$ J (7 MeV) range. In addition, the Van Allen belts contain also small amounts of ^{4}He nuclei and low energy heavier ions [13].

Similar radiation belts have been discovered around other planets with sufficiently large dipole magnetic moment. High radiation fields were identified near Jupiter, Saturn, and Uranus [14] associated with trapped radiation belts similar to Earth's belts. Jupiter's magnetosphere is very extensive. Its linear dimensions exceed the size of Earth's magnetosphere by 2 orders of magnitude. The front bow-shock is located at a distance of around 8 million km from Jupiter.

A.3 Space radiation effect

Effect of space radiation in matter

The CR interacts with matter through energy and impulse transfer processes. Energy transfer is accomplished especially by radiation interaction with electrons resulting in excited and ionized atoms or molecules. The high energy hadrons, leptons, and electromagnetic rays can interact with nuclei of targets with displacement from the equilibrium position. The deposited energy is quantified using absorbed dose (D) equal to absorbed energy per mass unit. The SI unit for D is $J \cdot kg^{-1}$ and is represented by the equivalent SI unit, Gray (Gy).

The value of D depends on radiation energy, mass and electronic densities of the absorbent material. Linear energy transfer (LET) is a significant aspect, especially in the microelectronics and biological damage effects evaluation. LET represent the energy transfer rate in irradiated target, expressed in terms of keV·μm^{-1} or MeV·μm^{-1}. Gamma, X and Beta rays have small LET values, while hadrons are associated with huge LET values.

For particle radiation, the absorbed dose is expressed as the product of the fluence of particles (the number per unit area), F, LET:

$$D = F \cdot LET$$

where F and LET are in the appropriate SI units.

In 2001 and 2003, Benghin *et al.* [15] determined the doses at multiple points of the International Space Station Russian Module during four solar proton events. The obtained values lie in the range 0.14-2 mGy/day. Through an inappropriate linear extension, these values correspond to 50.4 mGy/year and 730 mGy/year, respectively. Mewaldt *et al.* [16] reported a 500 mSv equivalent dose per year, corresponding to a D approximately 77 to 100 mGy/year.

For dose prediction in future human missions to the Mars, Mewaldt *et al.* [16] simulated D in the interplanetary space. The estimated D was in 60-160 mGy/year range, depending on solar activity. Huge values of cumulative D were reported in the case of long time exposure on deep-space missions [14]. These high values must be associated with radiation Jupiter's belts that were crossed during the space missions.

Radiation effects on electronic devices

The CR can affect electronics through three mechanisms [17, 18]: Total Ionizing Dose (*TID*), Displacement Damage (*DD*) and Single Event Effects (*SSEs*).

(i) *TID* has a cumulative physical dimension and depends on dose rate in the throughput space zone and exposure time for each space zone t_i, *i.e.*

$$TID(D) = \sum_i d_i \, t_i$$

(ii) *DD* is a non-ionizing energy loss (*NIEL*) and represents the change of the arrangement of the atoms in the crystalline lattice due to interaction between ionizing radiations and target nuclei. DD is generated especially by the hadrons components of the CRs. Leptons and electromagnetic rays with high energies have a lower contribution. The CRs damage effects in electronic devices was analyzed in ionizing doses and DD point of view. Liu *et al.* [19] analyzed the damage effects

induced by CRs in NPN bipolar junction transistors using the partial absorbed doses, ionizing dose D_i and displacement dose D_d, calculated as:

$$D_i = 1.6 \cdot 10^{-10} LET(x) \cdot \Phi$$
$$D_d = 1.6 \cdot 10^{-10} NIEL(x) \cdot \Phi$$

where $1.6 \cdot 10^{-10}$ is the unit conversion, x is the depth in the device (mm) and Φ is the incident particle flux.

Lu Ming *et al.* [20] evaluated the degradation induced by protons on triple-junction space solar cells and proposed a new method to determinate *NIEL* which can be used to calculate the corresponding displacement damage dose:

$$NIEL(E_0, \theta) = \frac{1}{x} \sum_{E_j = E_0}^{E_n} NIEL(E_j) \left[R(E_j) - R(E_{j+1}) \right]$$

where E_n is cutoff energy, θ is the angle between incident direction and the normal to the surface, R is the range of protons in materials and x is the thickness of the active region. Goiffon *et al.* [21] analysed the proton irradiation effects on increasing the CMOS image sensors dark current, and concludes that the *DD* contribution was negligible in comparison with the ionization effects.

(iii) *SEE*s are individual events which occur when an ionizing radiation transfer enough energy to cause a perceptible effect in a devices [22]. *SEE*s are generated by CRs with high LET value, like hadrons, and can take on many forms:

- Single-event upsets (SEUs) or transient radiation effects are software errors, non-destructive hard effects [23].
- Single-Event Latchup (SEL) identified in any chip with a parasitic PNPN structure and Single-event snapback, similar to SEL but not requiring the PNPN structure.
- Single-Event Transient (SET) represent de facto an electrostatic discharge through the electronic circuit.
- Single-Event induced Burnout (SEB) associated with high current and local overheating generation then may destroy the device.

B. Extreme temperature

The average temperature of the space is about 2.725 K, a theoretical expression of the cosmic background radiation, in other words, the energy still left over from the Big Bang [24]. Inside our solar system, there is a wide range of temperatures due to different distances from the Sun and local environmental conditions. The highest values were found near Sun in the specific case of Mercury

planet exposed surface, namely 738 K. On the opposite side are dwarf planets and outer planet's moons with 30-40 K surface temperatures [25]. Around Earth, temperatures range from 393 K for sun exposed surfaces to less than 90 K for unexposed surfaces [25].

For astronauts' spacewalks and Extra Vehicular Activities (EVAs), NASA reports that the bulky white spacesuits are subject up to 423 K difference from one side to the other. This can happen if an astronaut has one side of the suit facing the sun with the other side facing deep space. When continuously orbiting the sun, some bare metals can reach temperatures above 533 K; consequently, according to NASA'"to reduce the temperature hazards to astronauts performing EVAs, bare metals outside the Space Station and other spacecraft will have special coatings or blankets on them. These cautionary measures typically tend to keep "touch temperatures" between 400 K and 150 K".

C. High vacuum environment

The outer space vacuum can reaches pressures down to 10^{-14} Pa. In solar system, due to molecules accretion phenomenon induced by gravitational forces, the local pressures values have a relative large distribution. Fig. 2 shows vacuum pressure distribution in solar system reported by Miyoshi [26].
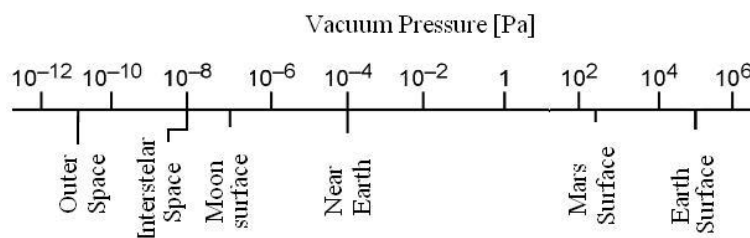
.

Fig. 2 – Average pressures in the solar system (reproduced with permission from [26]).

D. High velocity cosmic dust and micrometeorites

Cosmic dust and micro-meteoroids present another hazard to the operations of space vehicles. Operational spacecraft is continually exposed to collision with micro-meteoroids and space debris. As the space environment becomes more densely populated with space assets, the density of space debris of various sizes increases. Large space debris may have significant detrimental effects, as in the case of the Cerise spacecraft that had its 6-m boom vaporized by a space debris impact [27]. Very small orbital debris particles and micro-meteoroids are abundant; spacecraft surfaces returned to Earth have many small craters resulting from hypervelocity impacts. In most cases, these craters are too small to have any effect on the operation of the spacecraft. Some drastic events (*e.g.*, the total loss of the ESA Olympus

satellite in 1993 after an encounter with a meteor shower) prompted systematic studies of the micro-meteoroid effects in space. NASA's long duration exposure facility (LDEF) spacecraft was returned after approximately 5.7 years spent in low Earth orbit. Over 20,000 impacts have been documented on LDEF thus providing information on the micrometeoroid and orbital debris populations and their orbital distributions [28].

2.3.2. Evaluation of cosmic rays effects in condensed matter

For developing of space program, the effect of CR, especially in condensed matter, must by determined and quantified. The CR effects could be assayed by the direct evaluation of the effects in space and the simulation of space environment in laboratories on Earth.

Direct evaluation is restricted by cost and is limited at the determination of CR composition and energies using satellites and spacecrafts, the determination of D, E and biological effects on space stations (Skylab, MIR, ISS [15, 29, 30, 31] and manned spacecraft like Apollo program), the determination of satellite and spacecraft malfunction and the correlation with specific space environment conditions [32, 33].

The most of our knowledge on the CR effects is based on experiments performed using gamma sources [34], nuclear reactors [17] and particle accelerators [35–39]. Gamma (Co-60) and neutron sources (nuclear reactors and Cyclotrons) can be used especially for endurance testing on electronic devices. Simulation CR effects using low energy particles (below 50 MeV) are less relevant, especially for space radiation protection [40]. Using new accelerators, the ions with $1 < Z < 28$ should be accelerated up to energies in the range of 0.1–10 GeV/particle, around the energy spectrum of GCR.

An exceptional opportunity to boost research in this field comes from the construction of the laser-plasma accelerators [41]. This novel radiation sources will present unique opportunities for CR research, including the ability to produce a wide panel of particle species (gamma, electrons, protons, medium weight nuclei) with very high energies.

The ESA and NASA established space exploration programs for the coming decades, including long-term missions. Development of new programs implied evaluation of the potential CR effects to microelectronics, optoelectronics, electrical systems, sensors/ detectors, materials and astronaut crews. The proposal project aim is to simulate and quantify the space environment effects on condensed matter. The space stressors analysed in this proposal are: CR, extreme temperature and high vacuum pressure.

The main research areas are: dosimetry of radiation fields with similar characteristics with the CR, fundamental researches in the field area of energetic and

multi-component ionising radiation fields effect on condensed matter as well as effects of space environment on electronic devices, plastics and composite materials with applications in future space programs and endurance testing of experimental models and prototypes.

A. Dosimetry of radiation fields with similar characteristics with the CR

The complex radiation fields generated by interaction of 0.1-1 PW laser beam with specific targets must be characterised in terms of absorbed dose rate and total absorbed dose in condensed matter. Adsorbed dose will be quantified by:
- Determination of experimental radiochemical yields (standard chemical dosimeters like a Fricke ferrous-sulphate, cerium sulphate, free radical accumulation etc.)
- Inter-comparisons of obtained results due to complexes radiation fields generated by ELI NP facility and standard sources like Co-60 (using IFIN-HH DRMR, IRASM and INFLPR infrastructure)
- Calibration of commercial dosimetric films for specific ELI-NP radiation fields and use in experiments (using IFIN-HH, DRMR, and INFLPR infrastructure)

B. Fundamental research in the area of energetic and multi-component ionising radiation field effect on condensed matter

For understanding of the degradation phenomena, the fundamental processes in terms of radiation chemistry will be analysed. In this research direction will be assessed:
- Determination of active unstable chemical species (free radicals and activated molecules)
- Establish of the chemical fundamental processes in specific case of multicomponent and energetic ionising radiation fields

Determination of active unstable chemical species will be carried out using ESR spectrometer (determination of free radicals).

Establish of the chemical fundamental processes
Intermediate and final products can be determined using FTIR ATR, Raman and NMR spectrometers (in the ISO 17025/CNCAN accredited laboratories within IFIN-HH DRMR and IRASM) and GC MS, HPLC chromatographic techniques (in the ISO 17025/CNCAN accredited laboratories within IFIN-HH DRMR and IRASM). Experimental results will be inter-compared with obtained data using quantum-chemical simulations.

C. Effects of space environment on electronic devices, plastics and composite materials with applications in future space programs and endurance testing of experimental models and prototypes

The experiments consist of complex radiation fields exposure of targets, in a sealed vacuumed enclosure with a cryogenic and thermostatic mantle.

The CR will be simulated by complex radiation fields generated by interaction of 0.1-1 PW LASER beam with specific targets. The radiation fields will consist on electron (400-600 MeV maximum energy), protons (400-600 MeV maximum energy), gamma rays (approximately 400 MeV maximum energy) and, if is possible nucleus with $4 < Z < 14$ (approximately 400 MeV maximum energy).

Extreme temperature will be carried out using thermostatic mantle cooled with liquid He as cryostat agent (about 5 K) and heated with hot air (almost 800 K).

The proposed high vacuum pressure experimental condition is in the range of 10^{-4} to 10^{-6} Pa. Depending on the nature of irradiated targets and purposes, samples will be characterised using:

- Scanning electronic microscope (SEM) and Atomic Force Microscope (AFM) for identification of micro-structural changes (using INCDFM and IFIN-HH DFNA laboratories)
- Infrared spectrometer (FTIR) with Attenuated Total Reflectance (ATR) for identification of chemical modifications (using IFIN-HH DRMR and IRASM facilities)
- Mechanical testing post-irradiation facilities (using IFIN-HH IRASM laboratory)
- Functional characteristic in specific case of electronic devices and optoelectronics (external partners)

D. Degradation of optical crystals and solar cells in space

1. Objective

To use ELI-NP facilities for accelerated testing of the degradation of optical crystals and solar cells performance in space-like irradiation conditions. Beyond the scientific experiments, it can be thought as a testing service that ELI-NP can provide to manufactures of space solar cells or optical components designed to be used for satellites.

2. Physics case

Due to the high cost of direct investigations in space, the effects of cosmic radiation on condensed matter can be evaluated with ground based experiments and

ELI-NP facility is a very important candidate. Mainly because the high power lasers could be a better alternative for reproducing cosmic ray interaction with condensed matter, since the energy spectrum of laser accelerated particles is similar to the broad, multi-MeV-scale spectra of natural cosmic radiation, as opposed to the quasi-monoenergetic spectrum of particle beams in classical accelerators [41]. In the last years at the West University of Timisoara, the crystal growth group has gained an important experience in the field of growth and characterization of fluoride type crystals doped with rare earth elements [42, 43], while at the PV Laboratory an expertise in the monitoring, estimation and forecasting of PV systems operation has been developed (http://solar.physcis.uvt.ro). Therefore, an interesting topic that can be covered is the effect of radiation on solar cells, calcium fluorite and barium fluorite crystals.

Calcium fluoride (CaF_2) has much to offer as an optical material. Besides being highly transparent in the deep UV region, it also has excellent lifetime stability and relatively high damage threshold in the deep UV. Furthermore, CaF_2 has a broad transmission range, from 140 nm to 7.5 μm and beyond, featuring a low refractive index, removing the need for an anti-reflection coating. Therefore, CaF_2 optical windows are ideal for use as spectrophotometer windows. CaF_2 optical lenses are used in many spectroscopy applications used by NASA in CRISM and UCIS devices [44]. Likewise, CaF_2 grating prisms (grisms) have been successfully used in the NICMOS camera on board HST [45]. Barium fluoride crystal finds applications as a transmitting window over a wide wavelength range and as a fast scintillator involving emission at 195 nm and 220 nm, which is fairly temperature independent around 300 K [46], used for the detection of X-rays, gamma rays or other high energy particles. As it is one of the fastest scintillators known, it may be employed in outer space radiation detection devices. The damage of BaF_2 is caused by the formation of color centers, which cause a self-absorption of the scintillation light [47]. At the Crystal Growth Laboratory at the West University of Timisoara good optical quality CaF_2 and BaF_2 crystals can be obtained. For this reason, it is important to investigate how cosmic radiation exposure influences the defect structure and optical proprieties of such fluorides, as those employed in the manufacturing of optical components installed in space satellites.

On the other hand, the solar generator is the only spacecraft subsystem where electrically active semiconductor devices are directly exposed to space with a minimum protection. The most influential aspects of the space environment typically depend on the altitude and inclination of the mission orbit (the main operational

position of satellites are the geostationary orbit (GEO at 36 000 km) and the low-earth-orbit (LEO at several hundred km altitude with various inclination).

Trapped electrons and protons have the main contribution to the degradation of the solar cells efficiency. The main parameter in selection a space solar cell is the end-of-life (EOL) power output. A variety of novel devices and materials are under development world-wide: III-V compound solar cells comprising GaAs on Ge mono-, dual- and triple-junction devices (*e.g.* [48]). The current efficiency of the space solar cells is over 30% on space PV market and over 44% on research and development lab [49]. As example of solar cells degradation in space, the table below shows a comparison for the electrical performance for high efficiency silicon, dual-junction (2J) and triple-junction (3J) commercial space solar cells covered by thin glass film [50].

Table 1

Electrical performances for various space solar cells

Solar Cell Technology	Kg/m^2	η (%)		
		BOL	EOL GEO	EOL LEO
High- Efficiency Si	0.23	17.0	12.5	10.6
2J InGaP/GaAs-on-Ge	0.85	23.5	20.0	18.1
3J InGaP/GaAs/Ge-on-Ge	0.85	26.0	22.6	20.3

GEO Conditions (60°C) – 1-MeV, 5E14 e/cm^2
LEO Conditions (80°C) – 1-MeV, 1E15 e/cm^2

There are two main approaches for evaluating the solar cell degradation in space [51]. At the US Jet Propulsion Laboratory (JPL) the goal of the approach is the determination of the normal-incidence 1MeV electron fluence which produces the same level of damage to the cell as a specified space radiation environment. At the US Naval Research Laboratory (NRL), the approach is the calculation of the displacement damage dose for a given mission using the spectral damage coefficients and the proton and electron spectra incident on the cell.

E. Doped fluoride crystals irradiation for fundamental studies of optical properties modification

1. Objective

To use of laser plasma accelerated particle radiation from ELI-NP in order to study the change in optical and dielectric properties of irradiated crystalline materials with perspective novel laser applications.

2. Physics case

Interest on crystal growth and characterization at the West University of Timişoara, Faculty of Physics began 40 years ago. The *Crystal research laboratory - growth and characterization* is part of the Physics Department of the West University of Timişoara. The main goal has been to design set-ups and elaborate technology to obtain and to characterize the crystals. The participation of the WUT in the ELI collaboration will have a significant impact on the organization research in the field of crystal growth mainly at two levels:

- At the fundamental research level - the studies of material behavior in extreme environments (which is a central topic in the ELI-NP proposed experiments), will give a fundamental understanding of the radiation induced damage in crystals, taking advantage of the specific properties of laser driven radiation production, such as ultrashort time scale when the radiation is generated and the relatively broadband spectrum of radiation, complementary to the traditional nuclear physics research laboratories [41].

- At the applied research level – the experiments performed under high energy irradiation processes could be very helpful to obtain new laser materials for biomedical applications through crystal doping elements charge conversion radiation mechanisms.

The fluorides type single crystals are an important class of materials in the modern technologies of the solid state laser elaboration and radiation detectors. Rare earth doped CaF_2 and BaF_2 crystals are used as laser active media due to the well-known good optical properties of the fluoride host and due to the broadband transition of the different of rare earth ions used as dopants in the crystals. For example, the Er^{3+} ion properties have been intensively studied due to the its strong IR luminescence used for laser resurfacing of human skin [52] and the Yb^{2+} ions luminescence (around 314 nm) can be used in psoriasis phototherapy [53–55]. By doping CaF_2 and BaF_2 crystalline host with YbF_3, both Yb^{2+} and Yb^{3+} ions will coexists in the crystal. Yb^{2+} ions are responsible for emission in UV and VIS [56, 57] spectral domain and Yb^{3+} ions are responsible for the emission in near IR domain [58, 59].

Modification of ionization states of Yb^{3+} ions doped in CaF_2 crystals can take place due to γ ray irradiation [60]. Color center formation takes place after electron

irradiation [61]. Also, there exists a possibility that the site symmetry of the rare earth trivalent ions may change through radiation bombardment by electron or protons capture from the incoming radiation, which change the crystalline field around the dopant. Such formed rich multisite structure changes the crystalline field effects on the impurity ions, generating different electronic levels; some of these levels may be metastable and give rise to possibly useful laser applications. The proprieties of rare earth ions doped in CaF_2 and $CaBa_2$ after irradiation can be studied using optical and dielectric spectroscopy for the fundamental understanding of the defect structure formed after irradiation.

2.3.3 Laser-plasma acceleration of particles for radiation hardness testing

High-reliability, radiation-hardened and radiation-tolerant components and software are of vital importance in space applications, where satellite equipment implies much more complexity and miniaturization than before. In this context, the radiation environment used for ground testing should ideally be similar to the natural environment probed by the satellite, a condition which is difficult to achieve by traditional accelerator facilities. Recently, it was suggested that high power lasers could be a better alternative for testing applications [41], since the energy spectrum of laser accelerated particles is indeed rather similar to the natural one, as opposed to the quasi-mono-energetic spectrum of accelerated particle beams in classical accelerators. Moreover, additional advantages are related to the dimension of the ground experiment volume and the simultaneous availability of different radiation types. Our progress in filamentary plasma assisted laser acceleration of the electrons ensures better control of electron beams parameters (energy, intensity, spectrum, and divergence), by proper synchronization [62], duration, and intensity of the initial current in the filamentary plasma produced in different capillary configurations.

2.4 TESTING OF IRRADIATED OPTICAL COMPONENTS

With the advance of ultrashort and ultra-intense laser systems optical components are now placed in the vicinity of laser driven secondary radiation sources produced by the interaction of the laser with targets.

It is highly desirable to qualify the modification of the optical properties (reflectivity, transmission, absorption) as well as the damage threshold modification for the optical components exposed to such secondary radiation sources. ELI-NP will be a suitable place for studying such effects since at this facility a combination of many types of radiation will be generated simultaneously.

At INFLPR, which is located very close to ELI-NP, there is one of the very few laboratories in the world (ISOTEST) that can qualify the damage threshold of

optical components according to ISO standards.

ISOTEST Laboratory certifies that the Laser Induced Damage Threshold of a specific sample is tested according to recommendations of the ISO 21254-1,2,3,4:2011 standards. At the same time ISOTEST Laboratory can provide laser beam diagnosis. This kind of the laser beam diagnosis includes three types of measurements: measurement of the energetic characteristic (in the range of hundreds of nJ up to few J) of the laser beams, temporal characteristic (in the range of ns and tens of fs) and spatial characteristics of the laser beams. An arrangement set-up for the laser beam diagnosis is presented in Fig. 3.
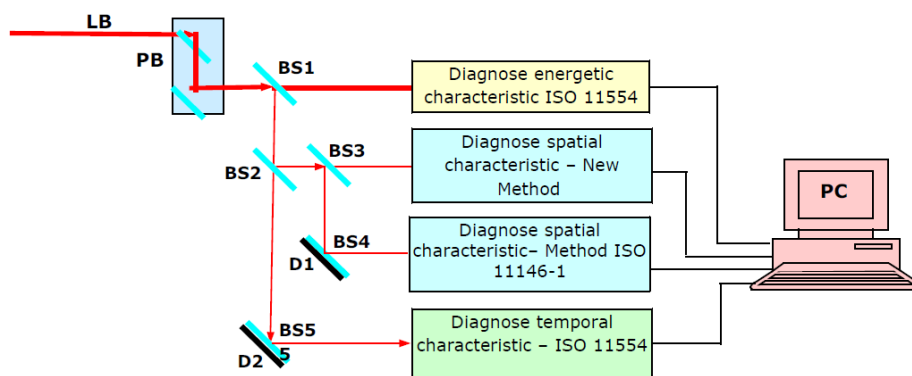
Fig. 3 – Experimental set-up for the laser beam diagnosis. **LB** – laser beam, **PB** – positioning beam (generally mirrors for testing the reflectivity, transmission, absorption), **BS 1,2,3,4,5** – beam splitters, **D 1,2** – dumpers, **PC**- personal computer.

The existence of ISOTEST and the specific needs of ELI-NP related to the qualification of the damage threshold of optical components in the vicinity of laser driven secondary radiation sources represents an excellent opportunity for this research direction at ELI-NP.

In the next paragraphs the ISOTEST capabilities of characterizing the optical surfaces in terms of damage threshold, for nanosecond laser pulses (Fig. 4) as well as femtosecond laser pulses are briefly described. The experimental set-up for S-on-1 procedure and feasability study executed with nanosecond laser pulses is shown in the figure below.
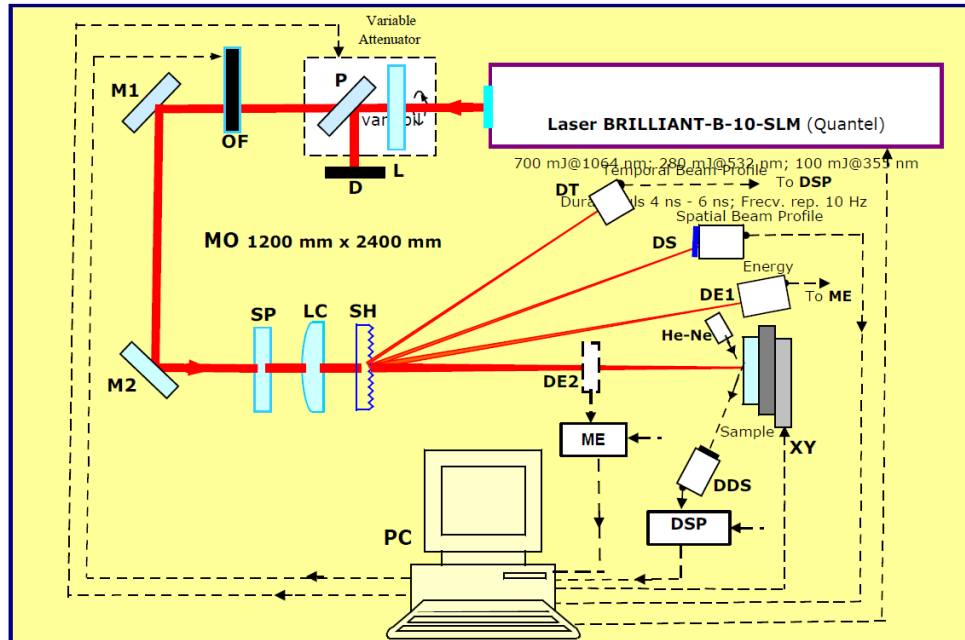
Fig. 4 – **L,** half wave plate; **P,** thin film polarizer at incident angle 45°; **D,** dumper for laser beam; **OF,** shatter for high energy laser beam; **M1; M2,** high reflectivity optical mirrors at 45° incident angle; **SP,** polarization selector: half wave plate; **LC,** convergent lens; **SH,** holografic beam splitter; **DT,** detector temporal beam profile; **DS,** detector spatial beam profile FireWare BeamPro model 2523; **DE1,** energy detector laser beam (measurement range 0,1 mJ – 10 J); **DE2,** energy detector laser beam (measurement range 0,005mJ – 2 J); **ME,** two channel energy monitoring; **DSP,** high speed digitizer (2 Gsa / s) of 10 bit, with high speed signal processor (FPGA structure); **XY,** motorised translation stage system for displacement and positioning the sample in the laser beam; **DDS,** detector damage sit: module photodiode C10439-03 with active aperture of 10 mm x 10 mm (HAMAMATSU) and lens with negative aperture; **PC,** personal computer.

Fig. 4 presents the architecture of the automated system for characterisation of the optical components and materials in the laser field. The laser beam delivered by a laser with emission in pulses of nanosecond and femtosecond pulse duration (with laser beam characteristic stable and reproducible) is set at the desired pulse energy by means of the variable attenuator controlled by the computer. Then the laser pulse is sent on the surface of the sample which is hold in the focal plane of the focusing system.

The sample is mounted on the multiple-axis (*xy*) micrometric system used for positioning the test -beam on the sites of the tested sample and also for the angle of incidence of the test-beam. The polarization state of the laser beam is set using a half wave plate or quarter wave plate. A small portion of the laser beam is diverted to the diagnose module, which simultaneously monitor the laser beam energy (in real

time), laser beam profile and the temporal beam profile. The spatial beam profile is monitored using a camera connected to the personal computer. The beam profile camera has attached a specialized software which estimates and calculates the effective area of the beam. The measurement plane of the spatial beam profile corresponds to the sample plane. The spatial beam profile of the laser beam measured with the beam profiler is identical with the spatial beam profile on the surface of the sample. The spatial beam profile is an important factor to determine the power density applied to the sample.

The temporal beam profile of the nanosecond laser is measured with a fast photodiode coupled through fiber optics to the oscilloscope. The electrical signal delivered by the photodiode is sent to the digital signal processor via the oscilloscope. The digital signal processor sends the information to the personal computer which commands the irradiation process. For the femtosecond laser, the temporal pulse duration is a lot more difficult because the time response of the electro-optic devices (photodiodes, oscilloscopes) is, in the best cases, in the range of picoseconds.

With the evolution of technology for ultrashort laser systems, some techniques and advanced devices (FROG, GRENOUILLE, SPIDER and WIZZLER) have been developed in order to determine the characteristics of femtosecond laser pulses in the time-frequency domain. These devices process the laser pulses and reconstruct with a very good accuracy the intensity temporal profile or the trace of the laser pulses. Temporal beam profile and pulse duration is very important for a correct evaluation of the power density of the ultrashort laser pulses applied on the sample, information which is essential in the ISO procedure.

In the cases of the procedures of the ISO measurement/diagnose of the ultrashort (fs range) laser pulses for the temporal beam profile and pulse duration an advanced device is used (FROG) which is coupled to the personal computer in order to control the irradiation process of the sample. The software which runs the entire procedure of the damage test is designed to control the movement of the sample along the x and y directions, to attenuate and to block the laser pulses, to count the site distribution and the number of pulses applied on each site until the damage has occurred. At the same time the software will detect the optical damage of the site exposed to the laser pulses. The software will also make a statistical analysis of the experimental data and it will calculate the damage probability of the tested sample versus the energy density of the laser pulse. After the automated measurement procedures, the software will automatically generate the measurement test report.

2.4.1 Pump-probe studies of optical surface damage using X-ray backlighting

In addition to the standard tests of laser irradiated optical components, we propose to develop and utilize a new diagnostic for the time-resolved study of

ultrafast laser optics damage. The motivation for this research is that the physical mechanisms for optics damage by ultraintense femtosecond lasers are still not well understood [63]. For instance, the post-irradiation experimental studies of femtosecond laser optics damage show consistently the formation of Laser-Induced Periodic Surface Structures (LIPSS), and of sub-µm scale roughness in the top layer of laser mirrors [64]. Better understanding of the laser damage mechanisms could lead firstly to the development of better optics, and secondly may enable developing techniques for early detection of dangerous conditions in the laser mirrors. In particular, there are almost no time-resolved studies of optics damage produced by femtosecond lasers [65].

The proposed technique consists in using grazing incidence illumination with a femtosecond X-ray backlighter, to measure in real-time sub-µm scale surface deformations and sub-surface electron density gradients induced by IR laser irradiation. The major advantage of using grazing incidence X-rays is that the scattering of electromagnetic radiation on micro-structures scales as $1/(\lambda^2 \sin\alpha)$, with λ the wavelength and α the grazing incidence (Fig. 1). For X-rays at grazing incidence ($\alpha < 0.01$ radian) the scattering is thus orders of magnitude more intense than for visible or IR light. As earlier observed, this may enable to non-destructively assess subsurface damage in optical materials using 1-10 keV X-rays [66].

The setup proposed to measure grazing incidence X-ray scattering is depicted in Fig. 5, and consists of a quasi-coherent (few µm size) X-ray backlighter emitting line or continuum radiation in the few keV range, followed by a Talbot grating interferometer. The probe X-ray beam is driven by a femtosecond IR beam split from the pump laser, delayable by an arbitrary time.

The Talbot interferometer enables measuring with very high sensitivity the ultra-small angle X-ray scattering (USAXS), caused by electron density inhomogeneities on the sub-µm scale [67]. Larger scale density gradients are also simultaneously measured through the phase change of the X-ray beam. X-ray interferometry with a betatron source backlighter was also proposed for real-time diagnostic of the electron density profile in accelerated solid targets in TDR1.

Two type of backlighters will be explored: (i) betatron emission from LWFA electron acceleration in gas [68], and (ii) K-α emission from laser heated nano-wire arrays [69]. Either of the backlighters can be driven by relatively modest power pulses (less than 100 TW), and are expected to emit bright and spatially coherent, femtosecond duration X-rays. The coherence can be improved using a third grating close to the backlighter. A HHG emission based XUV backlighter can also be considered.
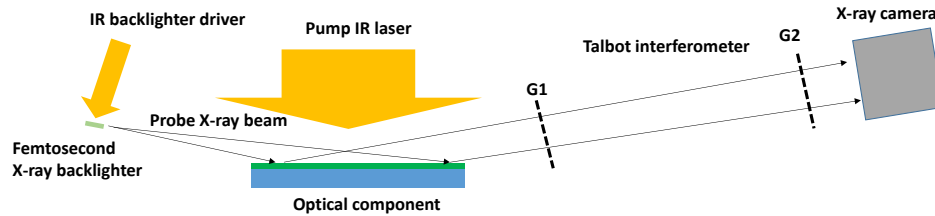
Fig. 5 – Layout of IR pump / X-ray probe diagnostic for time-resolved optical damage studies. G1 and G2 are μm-period transmission and absorption gratings, respectively.

The optical surface to be studied will be irradiated with a low intensity (less than 1 J/cm^2), large area IR beam, simulating the operating conditions of the mirrors at ELI-NP. The pump power density will be varied and its effects on the mirror surface measured in real-time, with μm spatial resolution. By varying the delay of the X-ray probe with respect to the IR pump it will be also possible to study the dynamics of damage formation. Lastly, another benefit of the proposed technique is that due to the grazing incidence of the X-rays, it will be possible to probe a large area (several cm^2 at least), in a single shot.

Using this method we hope to develop a predictive understanding of the laser damage mechanisms to the ELI-NP mirrors, and possibly a real-time method for detecting low damage levels, before they can compromise the mirror and subsequent optics.

2.5 Studies of materials for nuclear facilities

Energy production using fusion plasma is an expected goal and a research domain very well explored at the international level. In present the most reliable method to produce fusion nuclear reactions is those of the hot plasma, magnetically confined in a tokamak type reactor. The fusion device ITER (International Thermonuclear Experimental Reactor), to be operated at Cadarache, France is, probably the largest scientific project started ever. An important problem still unresolved is the material composition of the reactor main chamber (the first wall), materials to resist to the high energy fluxes of 10-100 MW/m^2. These energy fluxes appear during the plasma instabilities, when the magnetic field lines are losing the stable configuration and the ionized plasma particles having over 10 eV temperatures are directed toward the first wall. As instabilities examples we mention the edge localized modes (ELMs), disruptions, etc. Accordingly, for the wall protection was proposed to use tungsten plates in the divertor region, knowing the desired properties; low sputtering rate and the high melting temperature. The other materials are carbon (as form of CFC- carbon fiber composite) and beryllium (a light element

with a relative high melting temperature – 1551.15 K). However, the behavior of W, C and Be at high flux energies is not yet fully understood and is intensively investigated.

2.5.2 Direct laser irradiation of first wall materials

Preliminary experiments on direct exposure of first wall materials to fs laser have been performed. Irradiation of C, W and Be targets was performed by focusing an 800 nm femtosecond laser with the incident energy of 6.3 mJ, pulse duration of 70 fs at a repetition rate of 10 Hz on the target [70]. After irradiation the samples were investigated by means of SEM. Different morphologies of the irradiated areas were observed, depending on the target material (as seen in Fig. 6).
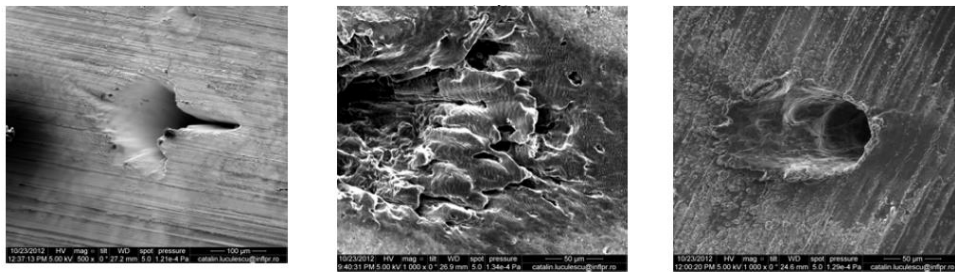
Fig. 6 – SEM image of a W sample after direct irradiation   SEM image of a C sample after direct irradiation   SEM image of a Be sample after direct irradiation

2.5.3 Laser-driven plasma effects on first wall materials

Indirect irradiation of solid targets has been performed, by producing plasma close to the target (femtosecond filamentation in air). The plasma-target interaction has been observed by SEM analysis of the samples as seen in Fig. 7 [70].
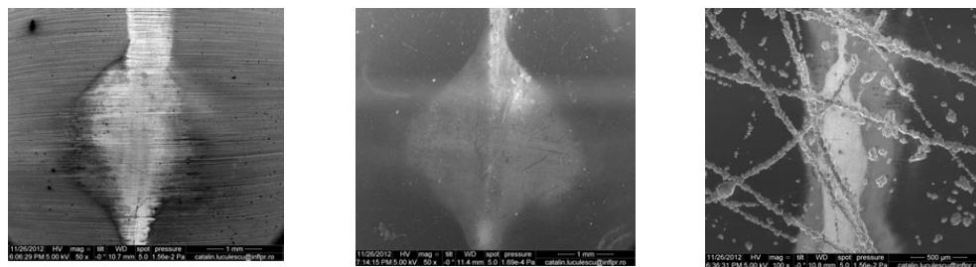
Fig. 7 – Plasma effect on the W sample.   Plasma effect on the C sample.   Plasma effect on the Be sample.

2.5.4 Periodic striations on Be and W surfaces by indirect femtosecond laser irradiation

As seen in Fig. 8, indirect laser irradiation of various samples led to periodic striations. We envisage that these types of experiments could be performed in the E4 experimental area by using the 100 TW femtosecond laser at a repetition rate of 10 Hz.
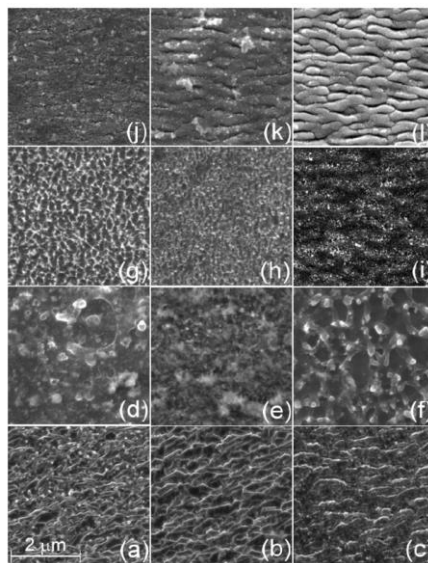

Fig. 8 – Exposed Be samples (images a-f) and W samples (images g-l) in air at atmospheric pressure after 1, 10, 30, 100, 300 and 1000 shots, respectively. (reproduced with permission from [71]).

2.6 BIOLOGICAL SYSTEMS UNDER IRRADIATION

The main objective of the proposed facility development described here is the investigation in the fields of bio-physics, radiobiology and biomedical studies, particularly the investigation of the interaction of biological systems with tunable multi-component, multi-energetic radiation, with relevance for improving biologic radioprotection in space missions, and for radiobiology studies with relevance in cancer treatment, especially for resistant cells, using the unique ELI-NP laser-generated radiation. The ELI-NP Experimental area E5 has the capability to operate two laser beams simultaneously and thus can provide two different types of radiation, some of them multi-component and multi-energetic, from solid or gaseous targets. The radiation beams can be superimposed on a biological sample or applied with a short delay between them to mimic the exposure to cosmic radiation.

2.6.1. Areas of biomedical research at ELI-NP

A. The impact of galactic cosmic radiation (GCR) on biological systems

The new experimental development will allow achievements that will provide a comprehensive scientific understanding of the effect of multi-component radiation on cells and organisms and an improvement of the biological radioprotection measures for astronauts in space mission, and for the airline crews.

The following objectives will be pursued:

- To establish an advanced "ground-based laboratory model" mimicking the complex high-energy and charge particle environment in space (GCR)

- To draw comprehensive biological networks of molecular events which might be altered by GCR, along with the corresponding repair-mechanisms

- To (re)classify the biological hazards due to space radiation exposure based on these molecular networks

- To identify molecular markers which underlie the biological susceptibility to the damaging effects of GCR, relevant for crew selection

- To develop biosensors for real-time biological monitoring of astronauts during space flight

- To (re)shape the biological radioprotection system for astronauts and air crews, taking into account the subtle functional changes possibly induced by repeated or long-term exposure to the complex, although low-dose cosmic radiation

- To develop therapies for preventing or counteracting the deleterious effects of chronic exposure to cosmic radiation.

B. Development of new approaches in biomedical and biomolecular studies for cancer treatment

The ELI-NP facility will have two 1 PW laser beams in the experimental area E5, which will further provide multi-component and multi-energy radiation beams. Thus it will have the capability to offer unique experimental conditions allowing biomedical studies which could deliver a new approach in cancer treatment and the associated medical technologies, to improve the efficacy by attacking cancer cells with highly targeted multi-component ionizing radiation and aiming to overcome the resistance to treatment of particular cancer cells.

The following objectives will be pursued:

– Using the high power laser at ELI-NP, to obtain highly-controlled and tunable multi-component radiation beams to be used for cellular and tissue irradiation

– To define at molecular level the mechanism of action of this complex radiation on normal and diseased cells/tissue, aiming to increase survival whilst reducing the treatment side effects by enhancing the radiation effect with nanoparticles

– To develop targeted theranostic strategies in cancer by joining this complex radiation approach with chemotherapy/immunotherapy and concomitant 3D imagistic monitoring of tumors

– To develop co-therapies for counteracting the deleterious action of the complex radiation, by specifically targeting the molecular events underlying the direct deleterious action of irradiation.

2.6.2. Motivations

A. Beyond state-of-the-art study

Due to the extensive space missions and current plans for permanent planetary bases, the issue of space radiation protection against Galactic Cosmic Rays (GCR), solar energetic particles (SEP), and trapped energetic particles in a planetary magnetic field, combined with a stressful microgravity environment, is becoming increasingly important.

GCRs consist of highly energetic nuclei, predominately protons and He, but also trace amounts of C, O, Ne, Si, Ca, and Fe ions. Particle energies can range from 100 MeV to 10 GeV per nucleon. Although the high charge and energy (HZE) nuclei are in trace amounts, they can cause more damage than protons, since they are more highly ionizing. Although typically being in the low-dose range, they are chronic and can significantly increase with solar events. Furthermore, GCR and SEP impinging on the shielding material, atmosphere, or surface of a planet can produce secondary radiation, including energetic neutrons [72].

This complex charged particle environment in space raises considerable challenges with regard to potential health consequences that can impact mission design and crew selection. The limited knowledge of the biological effects of different ions, in isolation and in combination, is a particular concern because the risk uncertainties are very high for both cancer and non-cancer late effects [73].

Although intensive research was done in this field, an obvious conclusion could not be drawn, mainly because the existing laboratory models of GCR were far from reflecting the complexity of charged particles in space, due to technological limitation. From the biological point of view, the published studies were only scattered parts of a complex puzzle, which could not be put together due to important experimental design differences at the level of radiation type, dose and irradiation geometry, cells and biological endpoints, etc).

Maalouf *et al.* [74] reviewed the knowledge evolution regarding the biological effects of space radiation on human cells, and the new investigations in this area of research are required by the complexity of spacecraft geometry and by the variety of used materials. Also the knowledge regarding the cellular response to complex radiation is fragmented and requires a comprehensive genomic and proteomic studies.

Regarding the exposure to low-dose radiation [74] this could be considered a useful model for the radiation environment of other planets with thinner atmospheres and weaker magnetic fields.

The ELI-NP facility will have the capability to respond to the challenge of generating a complex, multi-component and multi-energetic radiation which will closely mimic the GCR. We emphasize herein that synergistic biological effects of GCR components, along with thermal stress, hyper-oxygenation and microgravity, are expected. Therefore, to create such complex conditions at least at the level of a tightly controlled multi-component radiation is mandatory for obtaining reliable preclinical data regarding the biological effects of GCR on humans.

The ELI-emerging complex radiation will be modeled according to the data collected during space missions (World Data Center for Cosmic Rays) to mimic as realistic as possible the stressful conditions to which astronauts are exposed.

Preclinical investigations to be developed at ELI-NP and partner institutions, as part of a comprehensive molecular study [75, 76] using genomics and proteomics approaches will be performed such to:

- To document early and late health risks associated to chronic or repeated exposure to GCR, which may guide the evidence-based development of radioprotection measures, including new shielding materials and strategies.

- To discover specific biomarkers of susceptibility/resistance to GCR, which will sustain a medically rational selection of astronauts.

- To establish biological endpoints relevant for monitoring the exposed space crew (real-time monitoring during the space mission and long-term monitoring for potential late effects).

– To develop biosensors for real-time biologic monitoring of the space crew, which should be highly sensitive to molecular markers or processes which are altered rapidly by the ionizing radiation.

– To develop targeted therapies to counteract the deleterious action of GCR, by specifically addressing molecular networks responsible for the spreading of the damaging effects of ionizing radiation. In example, limitation of oxidative stress by transient activation of antioxidant elements transcription might provide protection against the damaging effects of GCR [77]. As shielding space radiation is seemingly quite challenging, the advances in biomedicine may reveal some more tools for radiation protection [78].

B. Exploring new approaches for improving treatment in cancer

Ionizing radiation is harmful in terms of risks to health, mainly due to its role as a carcinogen, but non-cancer effects were also recently demonstrated [79].

On the other side, ionizing radiation proved beneficial action in various diagnostic and therapeutic procedures in cancer (Table 2). Historically, there are three main types of irradiation: external beam irradiation or teletherapy; brachytherapy or sealed source irradiation, in which radiation is delivered internally inside or next to the diseased tissue; systemic radioisotope therapy or unsealed source irradiation, in which the radioisotopes are administered by infusion/oral ingestion.

Particle irradiation uses subatomic particles (electrons, protons, neutrons, carbon ions, alpha particles, and beta particles) to produce damaging ionization in tumor tissues. When a charged particle enters a medium the energy it deposits is approximately inversely proportional to the square of its velocity. Accordingly, as the particle slows, the probability of causing ionization events increases and a rapid accumulation of ionization events occurs in the irradiated tumor. The physical depth-dose distribution of particle beams in tissue is characterized by a small entrance dose and a distinct maximum (Bragg peak) near the end of range, with a sharp fall-off at the distal edge [80]. The particles have very little energy beyond the Bragg peak, which is seen at a tissue depth that is proportional to the energy of the particle [81]. Taking full advantage of the well-defined range and the small lateral beam spread, modern scanning beam systems allow delivery of the dose with millimeter precision.

Examples of particle irradiation treatments:

– Neutron beams are used for some cancers of the head, neck, prostate and for certain inoperable tumors. Because neutrons can damage DNA more than photons, effects on normal tissue can be more severe [82] but still show great promise in inoperable salivary gland cancers.

– Electron beams, produced by linear accelerators, are negatively charged, have a low energy level and do not penetrate deeply into the body. This type of radiation is used mostly to treat skin, tumors, and lymph nodes that are close to the surface of the body [83].

– Proton beams cause less damage to tissues, but are very good at killing cells at the end of their path. Therefore, proton beams are able to deliver more radiation to the tumor, whilst causing fewer side effects to normal tissues [84]. Protons therapy is used routinely for certain types of cancer, but it requires highly specialized equipment and is not widely available.

– Carbon ion radiation, are heavy particles which exhibit an enhanced biological effectiveness in the Bragg peak region, caused by the dense ionization of individual particle tracks, resulting in reduced cellular repair. This makes them particularly attractive for the treatment of radio-resistant tumors localized near organs at risk [85, 86]. This type of radiation is only available in a few centers in the world and is used in treating cancers that do not usually respond to radiation.

Table 2

Irradiation procedures and the corresponding delivery technologies

Technique	Delivery Technology
Image Guided Radiotherapy (IGRT)	2D IGRT, 3D IGRT, MRI guided IGRT
Intensity Modulated Radiotherapy (IMRT)	Linac based IMRT, VMAT, Tomotherapy
Stereotactic Radiation Treatment	Linac based SRS, Gamma Knife, Tomotherapy Cyber Knife
Advanced Imaging for Treatment Planning	4DCT, MRI – CT Fusion, PET – CT Fusion
Motion Management	Gated Radiotherapy, Tumor Tracking
Adaptive Radiotherapy	Adaptive Radiotherapy Procedures and Processes
Particle Therapy	3D Conformal Proton Therapy, Intensity Modulated Proton Therapy, Heavy Ion Therapy
Brachytherapy	Electronic Brachytherapy, Permanent LDR Implant, Directional LDR Permanent Brachytherapy

The irradiation technique proves to have important limitations, due to:

– Resistance to irradiation of particular cancer cells, mainly cancer stem cells (CSC) which are responsible for disease recurrence, having the exclusive ability to self-renew, differentiate into diverse type of progeny cancer cells, and initiate tumors [87]. Recently, it was shown that the irradiation itself can induce the development

of CSC [88]. The radio-resistance of CSC resides in enhanced repair mechanisms, upregulated cell cycle control and increased free radical scavenging. Moreover, CSC are apparently also involved in memorizing and spreading of radiation-induced genomic instability [89]. Protons preferentially target CSC and promising results were obtained by internal irradiation with ^{64}Cu-ATSM [90].

– Significant side-effects, more or less associated to the uncontrollable radiation-induced bystander and abscopal effects [91, 92]. The symptoms of late effects can be moderate-to-severe and show worsening over time, even 20–34 years after irradiation. These lesions often include fibrosis, tissue necrosis, atrophy, vascular damage and, in very severe cases, radiation-induced cancers [93].

Despite advanced treatment modalities, cancer still plagues us as a largely incurable disease, especially for the patients who detect the malignant neoplasm at a late stage. In addition, frequent metastasis and recurrence further frustrates even the best treatments currently available.

2.6.3. Proposed experimental investigations

A. Multi-modal irradiation approach

For responding to the need to overcome resistance to irradiation, taking into account the tumor intrinsic heterogeneity [94], we propose a research direction at ELI-NP that will investigate a novel strategy by multi-modal attack of cancer cells, with:

– Highly targeted and tunable multi-component, multi–energetic ionizing radiation, laser-generated, to be administered to the diseased tissue either successively or simultaneously, each component being efficient for destroying particular types of cancer cells within a heterogeneous tumor. This new approach has at least theoretically the potential to kill all types of cancer cells, but combination with chemotherapy is not excluded. Concomitantly, its multi-component nature raises the risk of important side-effects deriving from an increased dose delivered to the body.

   Therefore we should focus from the beginning on precisely targeting the irradiation, by using advanced imaging techniques for obtaining an accurate 3D image of the tumor to guide a clear-cut irradiation. For improving the imaging component of the multi-modal irradiation approach, biocompatible nanoparticles could be used as contrast agents, such as super-paramagnetic nanoparticles for MRI [95] or gold nanoparticles for X-ray imaging [96].

– Radio-sensitizers, for increasing the sensitivity of cancer cells to ionizing radiation, thus decreasing the irradiation dose and consequently the potential adverse effects [97].

Radio-sensitizations might be achieved by a) altering cancer cell metabolism (i.e. with nucleoside analogs); b) transient lowering of the antioxidant response of the tumor for sustaining the cytotoxic mechanisms of irradiation (oxidative stress).

We emphasize that nanoparticles which increase the power of existent imagistic methods, such as gold nanoparticles, were recently proved to have radiosensitizing properties [98].

– Radio-protectors, for limiting the effects of radiation-induced oxidative stress on normal tissues; recently, evidence exists that modification of key molecular targets to induce biological changes in the host can protect tissue from radiation damage.

– Immune-modulators, for protecting or reinforcing the host ability to fight against tumor cells, using conventional methods or emerging ones, such as intervention of the intestinal microbiota [99].

We emphasize herein that the very same nanoparticles used for improving tumor imaging, could be functionalized and used as drug carriers for radiosensitizers, chemotherapeutic agents and/or immunomodulators. Delivery through a carrier can significantly increase the efficacy of a drug by its tumor-specific targeting utilizing the enhanced permeability and retention effect [100].

Such a multi-modal irradiation strategy is a theranostic approach [101], joining imagistic and multi-modal treatment within a single procedure, which will allow for an efficacious personalized procedure [102] based on the patient's disease variant, characterized by a particular molecular profile of the patient and of the tumor. Besides the proof-of-concept-study, extensive molecular research should be done for assessing markers which will guide the selection of patients which will mostly benefit from this multi-modal strategy such as biomarkers which characterize the particular response of cells/tissues to the multi-modal irradiation (type of tumor cell death, repair mechanisms, response to oxidative stress) and biomarkers which define the susceptibility/resistance of various cancer and normal cells/tissues to this particular approach the impact of the multi-modal irradiation on the anti-tumor immune response, also taking into account that radiation-killed tumor cells might release tumor antigens which might trigger an efficient immune response against the tumor [103]. Such mechanistic studies will also draw the lines for developing co-therapies to counteract the deleterious effect of ionizing radiation in healthy tissue.

B. Molecular mechanisms underlying the deleterious action of radiation on biological systems

The molecular mechanisms involved in radiation-induced responses are complex, and multiple complementary approaches are needed to understand the overall reaction process.

Preclinical investigations in the above mentioned studies will go beyond conventional biomedical methods and procedures for toxicological/treatment efficacy assessments. We will take advantage of the latest technological and conceptual gains provided by proteomics [104] and genomics [105] to generate a large volume of data regarding the molecular basis of the biological effects exerted by ionizing radiation on a large panel of human cells, of cellular responses and individual susceptibility to this challenge. Data will be further integrated into complex biological pathways networks, which will be finally validated in animal models.

The extensive molecular study we are proposing aims to respond to challenging issues regarding the exposure to low-dose radiation, as defined in the Strategic Research Agenda of the Multidisciplinary European Low Dose Initiative (MELODI) [79] such as dose and dose rate dependence of cancer risk, non-cancer effects and individual radiation sensitivity.

The new experimental approach regarding biological effects of space-like radiation that will be developed at ELI-NP will bring innovation and valuable new preclinical data regarding potential synergistic effects exerted by a multi-component radiation, focusing on the molecular basis of the interaction and the corresponding cell/tissue response.

Important biomedical issues to be tackled at molecular level are [79]:

− The nature of the normal target cells for the radiation-induced deleterious effects (such as stem cells which may have specific responses to radiation and are thus involved in radiation-induced carcinogenesis).

− The contribution of DNA damage / mutational processes and epigenetic modifications (specific genes and genetic regulatory mechanisms can contribute to refining novel risk extrapolation models and the identification of radiation relevant biomarkers).

− The influence of cell micro-environmental and systemic processes, such as inflammatory reactions and effectiveness of both adaptive and immune surveillance.

− The molecular vehicles propagating radiation-triggered signals, such as soluble molecules (cytokines, oxidized molecules) and/or gap junction (by-stander effect [106, 107]).

− The nature of oxidative stress triggered in biological structures by radiation, its involvement in signal transduction [108] and cell/tissue functionality [109]; the specific anti-oxidant response developed by various types of cells following irradiation [110] which might a key element of individual resistance to irradiation.

   – The (epi)genomic profile which underlies the sensitivity of particular cells and individuals to ionizing radiation (whilst being a benefit in cancer treatment, radiosensitivity may be the cause of dramatic side-effects of even low dose-radiation).

By characterizing the molecular profile of the interaction between multi-component radiations and biological systems, valuable information will be obtained to foster the development of targeted therapies to counteract the deleterious action of ionizing radiation on normal tissues. Special emphasis will be given to subtle effects of low-dose radiation, which have apparently no immediate consequences, but which may alter homeostasis in the long-term and have important health consequences.

2.6.4. Multidisciplinary concerted approach

Such vast biological data can be obtained and integrated only by a sustained programmatic research effort, joining international expertise and state-of-the-art facilities for building a rational study based on concerted actions, unified protocols and a unique database.

By the very nature of the proposed research to be developed at ELI-NP and in partner institutions, multidisciplinary teams should be involved, joining at least the expertise of physicists, engineers, mathematicians, biologists, biochemists, biophysicist, physicians etc. ELI-NP should build the frame of multidisciplinary cooperation, by sustaining and promoting the dialogue between experts with various expertise.

3. TECHNICAL PROPOSAL

3.1. EXPERIMENTAL AREA

The experiments envisaged in this TDR will take place in the E5 experimental area, except the tests on the irradiated optical components which will take place in the E4 experimental area. In the figure below the two experimental areas (E4 and E5) are shown with respect to the laser room. E4 will host the two arms of the 0.1 PW laser with a repetition rate of 10 Hz, while in E5 the 1 PW lasers (25 J of energy with a pulse duration of 25 fs, at a repetition rate of 1 Hz) will be accommodated.

The experiments proposed at E5 will be irradiation of materials with secondary radiation beams for example electron beams, proton beams, neutron beams; we can foresee electron production by means of laser irradiation of gaseous targets and proton and neutron production by means of laser-solid targets interaction. A scheme

of an interaction chamber in E5 that will allow production of the above mentioned laser-driven secondary beams is shown below.
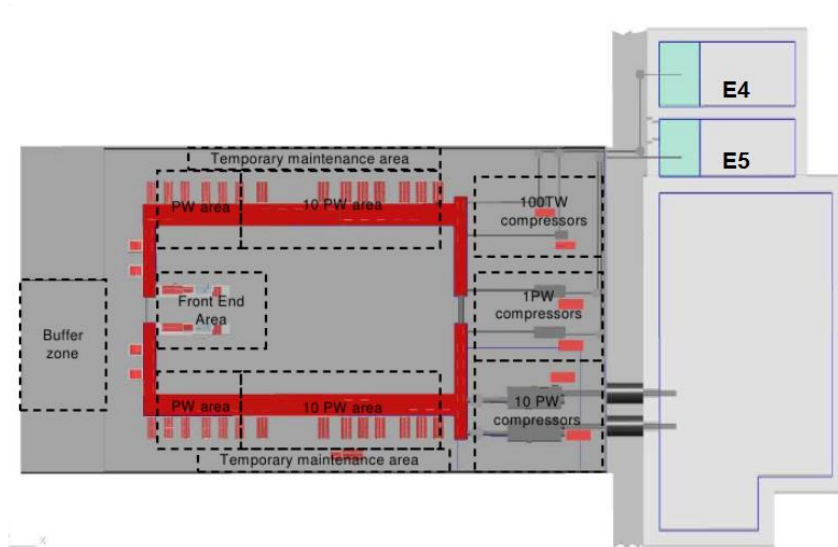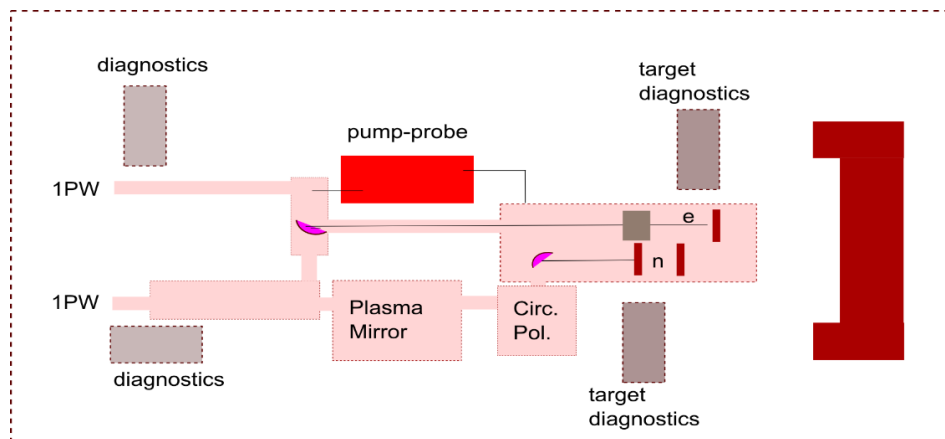

Fig. 9 – E4 and E5 experimental areas.

Fig. 10 – Schematic of a proposed interaction chamber in E5 for laser-driven secondary beams.

A CAD design of the experimental area E5 is shown in the figure below:
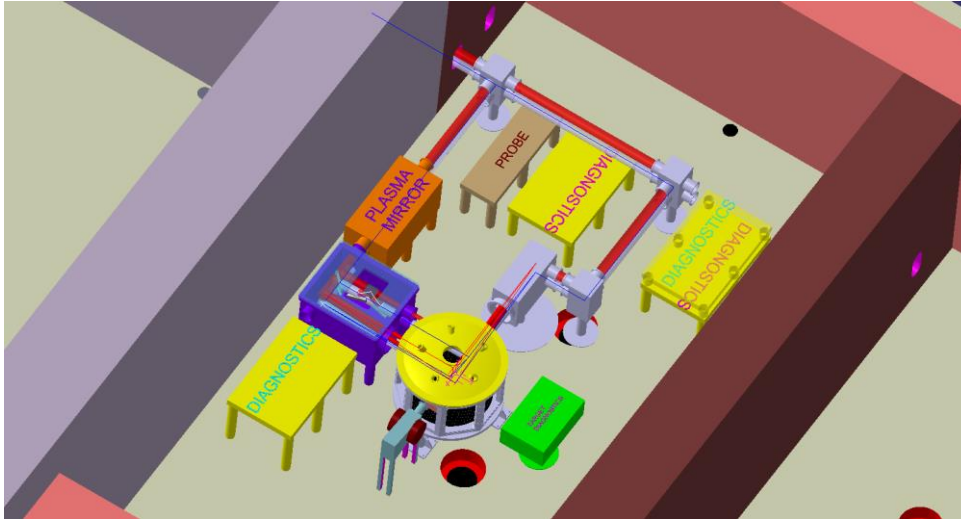

Fig. 11 – CAD design of E5 experimental area.

The ELI-NP E5 area will have the experiment monitoring and control systems architecture similar to the High Power Laser System of ELI-NP. The architecture is based on TANGO, which will permit local distributed control of the equipment and additional clients to remotely supervise/control the experiment.

This solution will allow a standardization of the control systems inside ELI-NP, while providing easy maintenance, better security, better logging and interfacing methods between the experimental area and the HPLS.

A dedicated UserRoom will be used to remotely control from outside the E5 area the equipment as the experiment is running. A TANGO framework will be developed to link the experimental area to the UserRoom using a dedicated client – server architecture that will allow maintenance and upgrades to be performed without interacting with other systems.

A data storage server will be available for short term experimental data saving and this shall benefit in general from dedicated data busses, separated from the client – server TANGO architecture that controls and monitors the equipment itself, in order to achieve the highest data throughput. Dedicated TANGO servers are envisaged to interface the equipment necessary in the experiment such as focal spot monitoring, solid target alignment, solid target manipulation, target insertion system, delay generators, monitoring CCDs and vacuum system for the E5 interaction chamber.

The above equipment will have a Human Machine Interface able to locally (from inside the interaction area) or remotely (from the user room) monitor and control the parameters needed to run the equipment and the experiment. Other equipment that do not allow an easy TANGO binding will be remotely controlled using its proprietary software through a remote desktop (or similar) connection. The user room will also provide to the users information regarding the HPLS parameters. However, the laser parameters will be controlled from the HPLS control room by the operators, from personnel and machine safety reasons.

3.1.1. Sample manipulation

For the experiments involving solid targets, the sample manipulation will be based on a load-lock system designed and developed in collaboration with the National Institute of Cryogenics and Isotopes ICSI Ramnicu Valcea. As seen in the figure below, the samples will be loaded on top of the chamber onto the *xyz* translation stage in the interaction chamber.
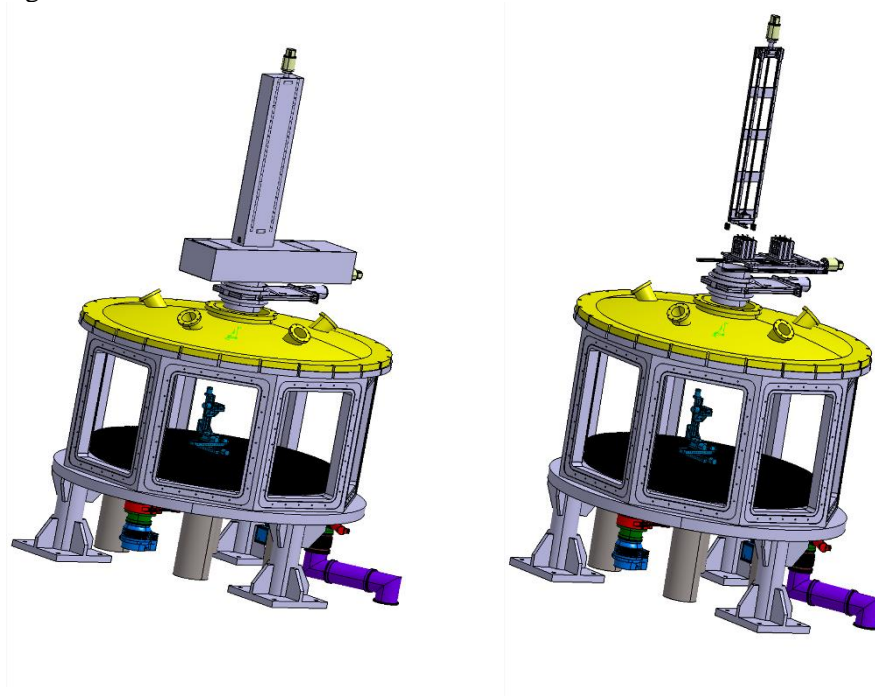

Fig. 12 – 3D CAD design of the load-lock system for solid targets manipulation.

3.2. OPTICAL SYSTEMS IN THE EXPERIMENTAL LAYOUT

3.2.1. Adaptive optics and circular polarization system

The Adaptive Optics and Circular Polarization System provides two functionalities. Firstly, the Adaptive Optics System has the purpose of optimizing the wavefront quality and also compensates for the gravitational effects that affect the mirrors. Secondly, the Circular Polarization System transforms the P-linear polarized input beam in a circularly polarized beam, with fine tuning of the polarization ellipticity from 55 degree to 81.5 degree at 820 nm central wavelength, while providing collinear input and output laser beams. The circular polarization of the beam is particularly suited for radiation pressure acceleration (RPA) experiments. A CAD model of the implemented system is shown in the figure below.
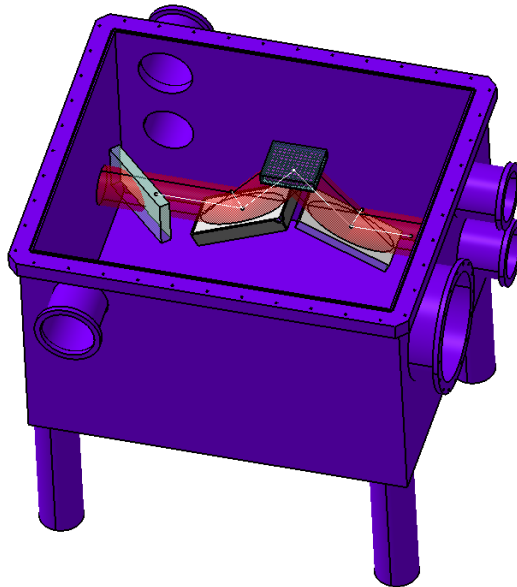

Fig. 13 – CAD model of the implemented adaptive optics and circular polarization system in E5.

For a reflective polarization control system, reference descriptions exist in literature [111, 112]. However, the systems described in the above mentioned references generate a circularly polarized beam without controlling the degree of polarization. The Polarization Control system of ELI-NP provides the control of the degree of polarization, using reflective mirrors, while maintaining the collinearity of the input and output laser beams. The configuration of the system is shown in Fig. 13. It consists of two plane mirrors (M1 and M2) and one deformable mirror (AO).

A rotating system with the rotating axis collinear with the axis determined by the direction of the laser beam propagation (in red color, Fig. 14) will allow the rotation of the mirrors along the laser beam axis.
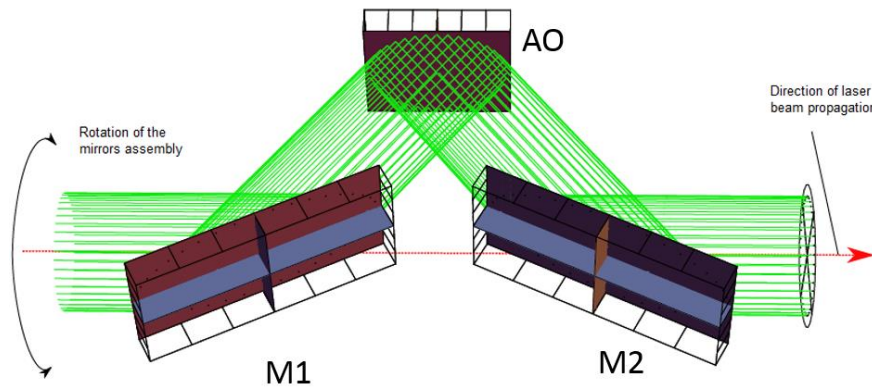

Fig. 14 – Side view of the circular polarization system.

The first plane mirror (M1) has one degree of freedom (rotation, as seen in Fig. 14), while the second one (M2) has both translation and rotation. The deformable mirror (AO) has one degree of freedom for translation hence allowing fine tuning of the degree of ellipticity.
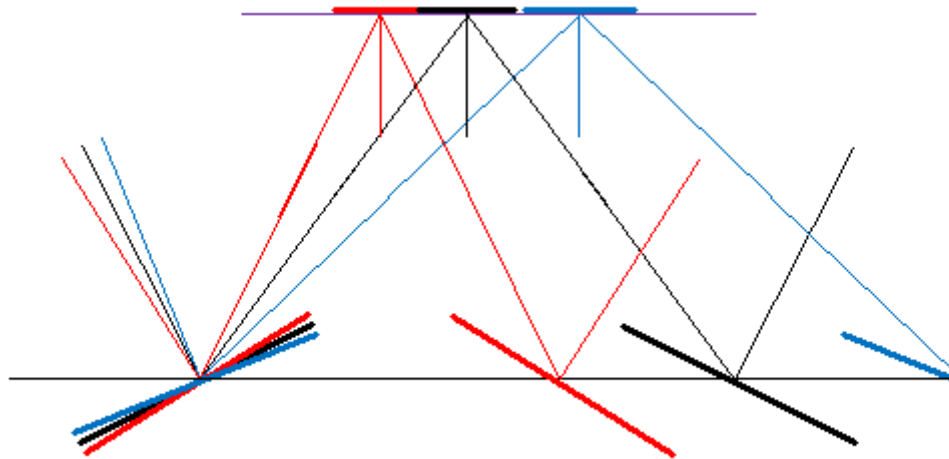

Fig. 15 – Schematic view of the system along the laser propagation direction, showing its working principle.

3.2.2. Plasma mirror system

In order to improve the temporal contrast of the 1 PW laser pulse after the compressor, a double plasma mirror system will be used, as schematically shown in the figure below.
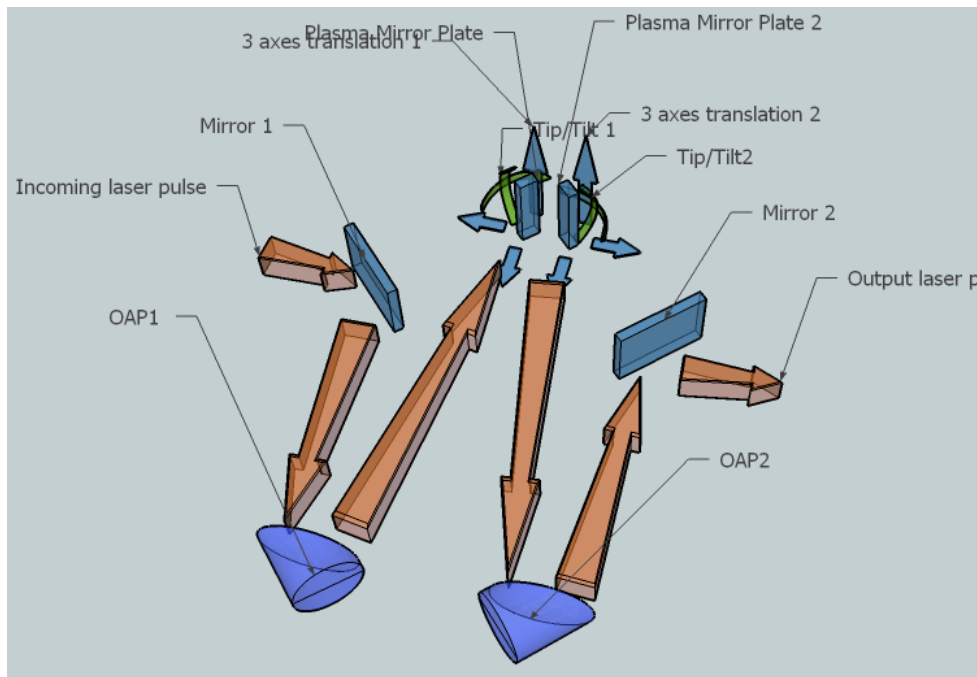

Fig. 16 – Schematic of a double plasma mirror system to be used in the E5 experimental room.

With such a system a high contrast of 10^{11} was achieved at 6 ps before the main pulse [113]. The double PM scheme is composed of two flat mirrors, two off-axis parabolic mirrors and two dielectric plates with antireflection (AR) coating. The off-axis parabolic mirror (F/10) will be designed for an angle of incidence of 5 degrees.

The two dielectric plates acting as plasma mirrors will be accommodated in a separate vacuum chamber. Typically, the improvement of contrast is around 2 orders of magnitude for one dielectric plate with AR coating.

3.3. LASER TARGET INTERACTION

3.3.1. Laser wakefield electron acceleration (gaseous targets)

Laser produced plasmas, as a result of the interaction between a high power laser and a gas target, can produce high electric fields in the order of hundreds of GV/m which are a few order of magnitudes higher than the fields in the classical accelerators. Hence, one can envisage that electrons could be accelerated in this fashion to relativistic energies.

The first indication that this could be the case came in 1979 [114], when it was shown that plasma waves can accelerate electrons due to the ponderomotive force of the laser. The plasma waves created by the laser pulse propagate close to the speed of light behind the laser pulse. In the case of large amplitude plasma waves, the electrons in the plasma can be trapped and accelerated by the longitudinal electric fields of the waves (wakefields) to high energies as schematically shown in Fig. 17.

The first observed energetic electron beams from laser wakefield acceleration were produced by picosecond laser pulses [115, 116] and had a Maxwellian spectrum. About a decade later the first mono-energetic beams of relativistic electrons were produced using laser pulses with less than 100 fs pulse duration and with energies from 60 to 170 MeV [117–119].
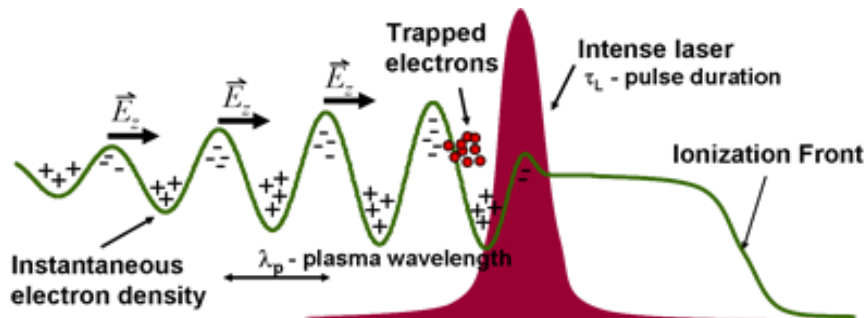

Fig. 17 – Schematic of the interaction of a laser pulse with a neutral, low atomic number gas.

In 2006 the first beam of accelerated electrons with 1 GeV energy was reported [120] by channelling a 40 TW peak-power laser pulse in a 3.3-cm-long gas-filled capillary discharge waveguide.

Current state-of-the art in the electron beam production by means of PW lasers include the acceleration of quasi-monoenergetic electrons to 2 GeV [121] as well as the acceleration of electrons up to 3 GeV by means of dual-stage laser-wakefield acceleration [122]. We envisage that for our experiments the energy of electrons will be in the range of 0.5 to 1 GeV, with a maximum energy (from a radioprotection point of view) of 2 GeV.

3.3.2. Laser driven proton beams optimized for pump-probe experiments

Most experimental research so far in the area of laser driven ion acceleration has been dealt with the target normal sheath acceleration (TNSA) mechanism, where ions are accelerated by space charge fields set up by relativistic electrons at the target surfaces. After only a short period of development, TNSA ion beams have been shown to have several properties, such as brightness, laminarity and pulse duration, markedly different from those of conventional accelerator beams [123]. Such beam parameters are suitable for various pump/probe experiments in an ultrafast timescale, which is not feasible while using ion beams driven by conventional accelerators. Although several other laser driven acceleration mechanisms, such as Radiation pressure acceleration (RPA) [124], Breakout afterburner (BOA) [125], are currently being explored, TNSA mechanism stands as a robust acceleration mechanism for incident laser intensity up to 10^{20}-10^{21} W/cm^2. Recent experimental results obtained with petawatt class lasers shows acceleration of protons in excess of 30 MeV [126, 127], which is significantly higher than that required for the planned irradiation experiments. The TNSA mechanism offers flexibility of tuning proton energy by varying various laser and target parameters. For instance, reducing the laser intensity on the target by a factor of 4, either by increasing the focal spot size on the target or by increasing the laser pulse duration, will lead to factor of 2 drop in the proton energy, bringing the proton energy close to the required value, without sacrificing the laser-to-proton conversion efficiency (which in turn implies a commensurate increase in proton number while decreasing the proton energy) [128].

TNSA driven proton beam is an extremely suitable candidate for probing highly transient phenomena with ps temporal and micron spatial resolutions. Where the micrometre scale source size of the protons (due to the micrometre scale focal spot size of the intense laser on the target) allows 2D radiograph of an object to be taken in a point-projection imaging scheme, broad energy spectrum of the source provide multi-frame probing capability due to different time of flights of different energy protons arriving at the probed object [129]. Proton radiography is a well-established diagnostics used in the laser plasma interaction experiments to study underlying physical mechanisms by mapping, spatially and temporally, the evolution of transient electric and magnetic fields associated with the interaction. Proton radiography is also suitable for studying small density variation across a probed object due to small-angle scattering of protons sensitive to material type and density [130]. With the dual pulse capability of the E5 experimental area, the proton beams from one of the arms can be deployed on demand for radiography of the sample being treated by the second arm.
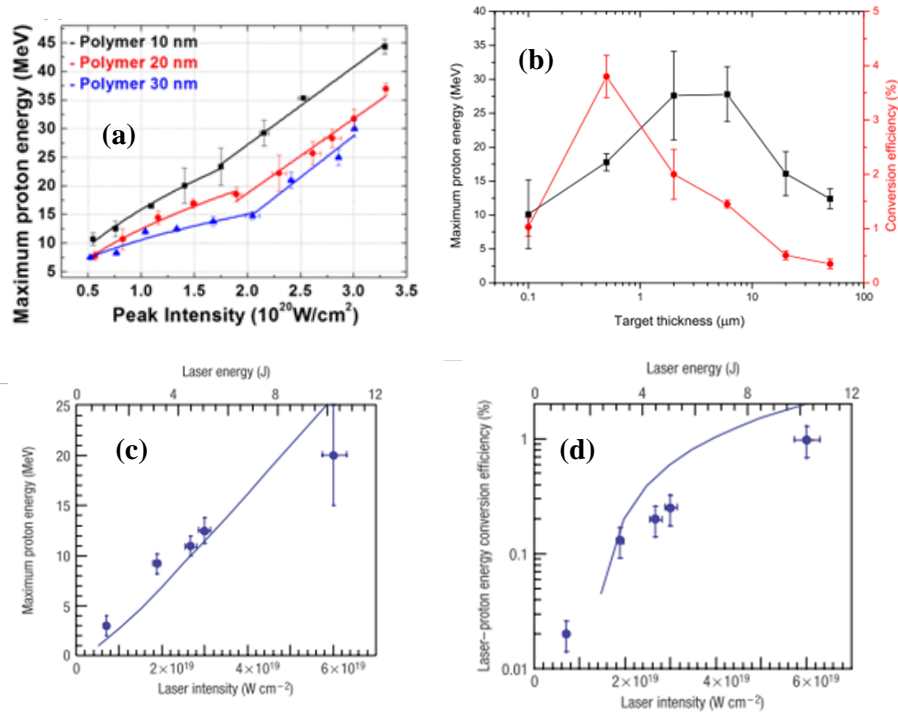
Fig. 18 – Graphs (a) and (b) show the recent experimental data on maximum proton energy produced from the interaction of petawatt class laser with thin foils. (c) and (d) show previously reported scaling for proton energy and conversion efficiency with respect to laser intensity and energy (reproduced with permission from [126, 127]).

Although the proton energy and brilliance at the source match the requirement of the irradiation experiments, the broad spectrum and large divergence of the proton beam requires additional method for beam control. The manipulation of laser generated proton beams presents specific challenges due to the high bunch charge and short pulse nature of the beams. Therefore innovative approaches are required to enable beam control and optimisation. In order to deliver a narrow energy band proton beam of high flux, at a reasonable working distance of 10s of cm from the laser irradiated target (to provide adequate space for shielding of the test sample), a novel target geometry as shown in the Fig. 19(a) will be deployed. The target contains a proton generating foil, of material and thickness as best suited for the given laser parameters, attached to the front of a helical coil structure made of a thin wire. The helical coil provides a unique conducting path for the flow of electron to the target in order to compensate the impulsive loss of electrons during intense laser interaction with the proton generating foil.
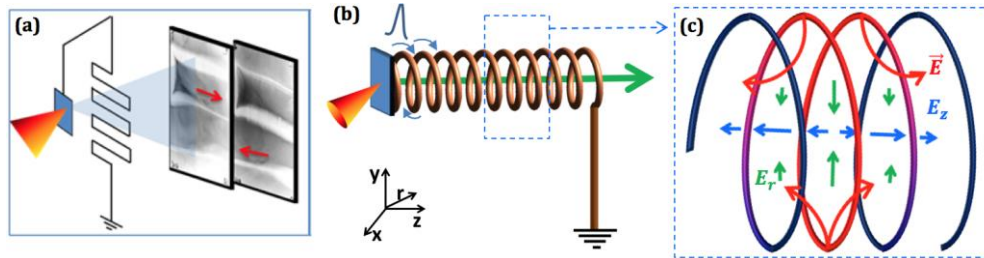
Fig. 19 – (a) Shows the setup and data obtained characterizing the charge pulse flowing along a wire connected to the laser irradiated target. (b) Schematic of the target designed for controlling beam parameters of laser driven protons. The helical coil design allows the charge pulse to flow around the proton beam axis, which results in affecting protons of a given range of energies, travelling synchronously with the charge pulse. A schematic snapshot of a small section in the coil is shown in (c) which shows the electric field configuration inside the coil. The red part of the coil represents the segment charged by the travelling pulse at a given moment of time. Where the red arrows represent the electric field lines originating from the coil, the green and blue arrows represent the radial and longitudinal components of the electric field respectively. The length of the green and blue arrows represents relative strength of the field at different locations.

Due to the extremely transient nature of the charging of the laser irradiated target [131], the neutralising current flow along the wire of the helical coil as a localised pulse, moving with a speed close to the speed of light in vacuum. Due to the use of thin wires, the linear charge density associated with the pulse produces strong electric field around the wire capable of deflecting MeV protons, as shown in the proton radiographs of the charged wires taken by MeV protons (see Fig. 19a). The helical target geometry aims to employ this field for simultaneous focussing, energy selection and post-acceleration of MeV protons, by allowing the charge pulse to travel in a helical path around the proton beam axis, as shown by the schematic in Fig.19b. The effective longitudinal velocity of the associated electric field pulse is determined by the coil geometry, and, with an appropriate choice of parameters (e.g. coil diameter and pitch), the field can co-move with a desired section of the TNSA proton spectrum, over an extended propagation length. In this configuration, the radial and longitudinal components of the electric field act, respectively, towards focussing and further acceleration of the co-moving protons (or deceleration for the protons lagging behind the charge pulse).

For an illustration, Fig. 20 shows a typical data obtained at the in-house TARANIS laser (10 TW CPA laser delivering intensity of a few times 10^{19} W/cm^2 on target) facility at the Queen's University Belfast (QUB). The foil-coil target in this case has produced a highly collimated/focussed beam of protons, with a commensurate (nearly an order of magnitude) enhancement of proton flux, in comparison to the typical divergent proton beam produced by a normal flat foil. By varying the radius and pitch of the coil, the flow of the charge pulse was synchronized with different ranges of proton energies, resulting in focused beams of different energies. The unsynchronized protons in this case maintain their intrinsic

divergence, which will allow spectral tailoring by using a spatial aperture at a far distance from the target.
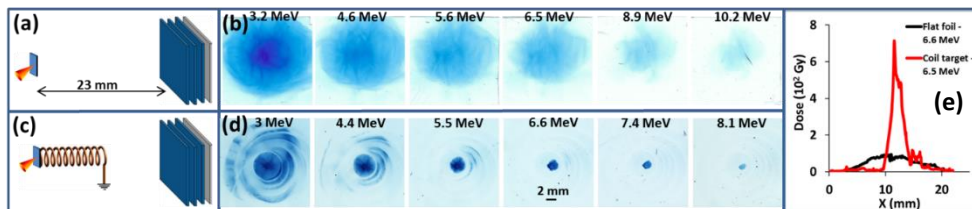

Fig. 20 – (a) and (c) shows the schematic of the experimental setups for the reference flat foil and the proposed coil target respectively. (b) and (d) shows the proton beam profile obtained over different layers of detectors (corresponding to different beam energy) for the case (a) and (c) respectively. **(e)** shows the comparison between the horizontal lineouts across the proton beams obtained in the 4th layer of (b) and (d).

The peak charge density/current in the wire depends on hot electron temperature and flux, which in turn depends on the intensity and energy of the incident laser pulse. Therefore one can expect a significant increase in electric field strength inside the helical coil while using this technique at the E5 target area equipped with Petawatt laser.

Experimental Plan:

The helical coil targetry is made of thin metal wires (approximately 100 μm diameter) winded into the shape of a helix, where the diameter and pitch is chosen as per the required beam output. For example, a helical coil of mm-sized diameter, few hundreds of μm pitch and a few cm long is suitable for generating a pencil beam 10-20 MeV protons, which is the desired energy range for most of the planned experiments in the E4 and E5 target areas. Being connected directly to the rear of the proton generating target, the "foil+coil" assembly stands up as a single target which provides greater flexibility in terms of target deployment and alignment. A number of "foil+coil" targets can be mounted on a translational/rotational stage for shooting at a fast repetition, without the need for breaking the vacuum of the interaction chamber. The coil targets will be mass-manufactured with high precision and reproducibility, and will be provided by QUB.

Since TNSA acceleration is not prone to low contrast of laser, as long as a suitable thickness of the proton generating foil is chosen (typically a few μm up to 10 μm, depending on the laser), one could benefit in terms of proton energy and flux by bypassing the lossy plasma mirror system. Due to the compactness of the target, the multi-target stage can be easily fielded inside the interaction chambers at E5 target area. The targets can be aligned in the same way as one would do so for simple

flat foil targets. The output beam from the coil targets is highly collimated (less than 0.5 degrees divergence), which mitigates the technical and radiation issues associated with setting a secondary target in a close proximity to the primary proton generating target. The pointing of the proton beam exiting the coil target solely depends on the axis of the coil, which can be controlled with micron precision. Therefore, one could simply use an appropriate shielding in between the primary and secondary targets, with a sub-mm pinhole aperture for the proton beam to pass through. Due to extremely low divergence of the proton beam, the secondary target can be placed several tens of cm from the coil target, which will provide enough room for using a thick shielding of high Z material in order to reduce significantly the exposure of other intense radiations, such as X-rays, produced by the laser plasma interaction. In order to assure a cleaner irradiation environment, one can also use a setup as shown in the Fig. 21. In this case, a pair of strong magnets (approximately 1T) can be used to steer the pencil beam of protons exiting the coil target by a small angle as adequate for blocking the direct line of sight between the sample and the laser interaction point. The proton flux on the sample will not be compromised in this case because of the low divergence and energy bandwidth of the beam produced by the coil targets.
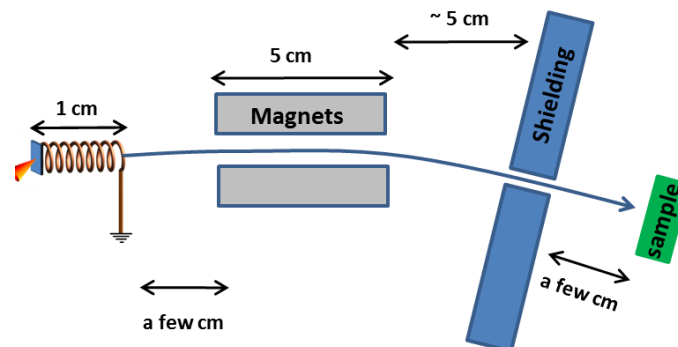

Fig. 21 – A schematic (not to scale) of the experimental setup using magnets to steer the pencil beam of narrow energy bandwidth protons coming out of the coil target. In this case the shielding can be placed obliquely in order to obscure the direct line of sight from the laser interaction. This setup will therefore allow an extremely clean irradiation environment. Tentative dimensions and separation between different objects are mentioned.

3.3.3. Neutron production from secondary protons

Over the past decade, significant attention has been paid to laser driven sources capable of producing short neutron bursts due to the advantages in terms of cost reduction and compactness, reduction of radioactive pollution and ability of radiation

confinement by closely-coupled experiments. Among the possible laser energised nuclear phenomena, the most established route to create a neutron source is employing laser accelerated ions in either fusion or spallation reactions. Since spallation reactions require high energy projectile ions, fusion reactions based on low atomic mass nuclei, such as ^{7}Li(p,n)^{7}Be, ^{9}Be(p,n)^{9}B, ^{13}C(p,n)^{13}N, d(d,n)^{3}He, T(d,n)^{4}He, ^{7}Li(d,xn), ^{7}Be(d,xn), are particularly relevant. The neutron yield from fusion reactions scales with the product of fusing ion densities and cross-section σ, which for most common reactions reaches high values for centre-of-mass energy in MeV range (see Fig. 23). Such a source is expected to provide not only a short initial pulse width (in sub-nanosecond range), but also a narrow band energy spectrum so that the pulse duration is maintained over a reasonable distance from the source.
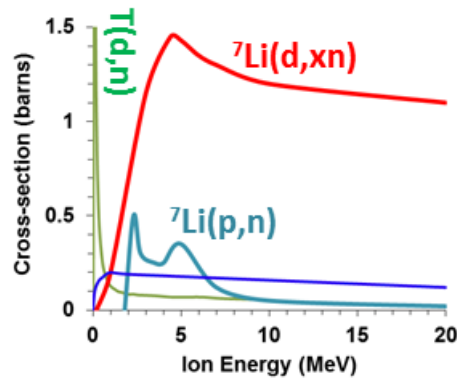

Fig. 22 – Comparison between cross-sections of a few fusionreactions. D-D reaction have high yield for sub-MeV ions, D-low Z reaction have significantly high yield for higher ion energies.
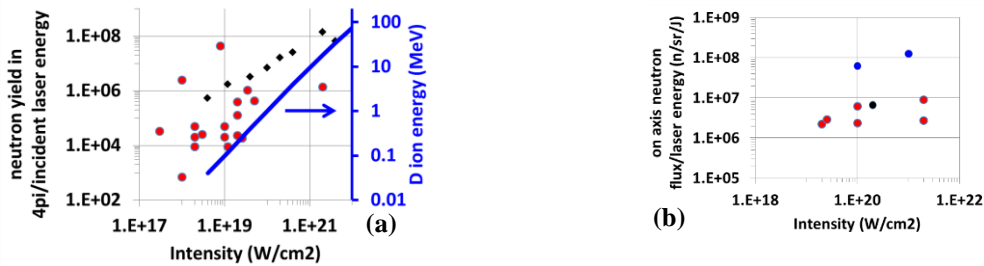

Fig. 23 – (a) In-target Fusion: Experimentally obtained neutron yields [133, 134, 135, 136, 137, 138, 139, 140, 141, 142, 143, 144, 145] (red circles) collected from literature for vs. estimated (black) neutron yield at different laser intensities is shown. Increase in deuterium ion energy from the front surface of a solid deuterated plastic foil, driven by hole-boring mechanism, with increase in laser intensity is shown as blue solid line. (b) Pitcher-catcher setup: Experimentally obtained on-axis neutron flux collected from literature as a function of laser intensity. Red, black and blue dots shows the data obtained for TNSA driven proton and deuterium ions on Li Catcher [145, 146, 147, 148, 149], TNSA driven deuterium ions on deuterium catcher [150] and BOA driven deuterium ions on Cu and Be catcher [151].

Producing high flux of MeV ions using intense lasers is currently an area of intense research [123]. Where a number of emerging ion acceleration mechanisms, such as Radiation Pressure acceleration (RPA) [124] and Breakout afterburner (BOA) [125], hold the promise for producing higher energy ions with higher efficiency, Target Normal Sheath acceleration (TNSA) is a well-established and robust mechanism which produces MeV ions with high flux and narrow divergence. Such beams can be readily deployed in a pitcher-catcher setting for neutron generation via beam-fusion reactions. Alternatively, dense bunches of MeV ions from the target front surface, driven by intense laser in so-called 'hole-boring' regime [132], can efficiently generate fusion neutrons by colliding, as they propagate through the target, with the cold ions in the target bulk. In the hole-boring process, directional momentum transfer from laser to target ions via radiation pressure acts as a snowplow on the target front surface, and launches a dense ion bunch into the target. For a semi-infinite target, the energy gain per ion scales directly with the laser intensity and inversely with target mass density. Therefore, for what concerns the achievable neutron yield, both schemes are equally promising for the intense lasers available at E4 and E5 target areas.

Considering a simple geometry of beam-fusion column, neutron yield can be written as, $Y = N_{ion}\rho_{bulk} < \sigma v > \tau_{burn}$, where, N_{ion} is the number of ions propagating in a medium of density ρ_{bulk}, $< \sigma v >$ is the velocity averaged fusion reactivity and τ_{burn} is the fusion burn time – i.e. the propagation time of the ions inside the medium. Therefore, using high flux of energetic ions from the laser driven sources will increases the neutron yield significantly, not only due to the parameters N_{ion} and $< \sigma v >$ in the above formula, but also due to the increase in the fusion burn time by deeper penetration of higher energy ions into the neutron converter. Fig. 23 shows the neutron yield reported in literature from both the cases, which increases with increasing laser intensity on target.

In addition to the benefit of high fusion cross-section, anisotropy in neutron emission is another facet of the beam-fusion reaction. For example, simulations [152] show that using several MeV deuterium ions in D-D reaction yields a neutron flux strongly peaked along the ion beam forward direction, and that the anisotropy grows further with increase in ion beam energy. The anisotropic emission of the neutron beam is starting to be realized in experiments as shown in the Fig. 24, which, together with high flux, provides a suitable basis for pump/probe applications. With the intense laser available at E4 and E5 target area, it would be possible to attain significantly higher ion energies, which would most likely provide better neutron beam parameters for the irradiation experiment.
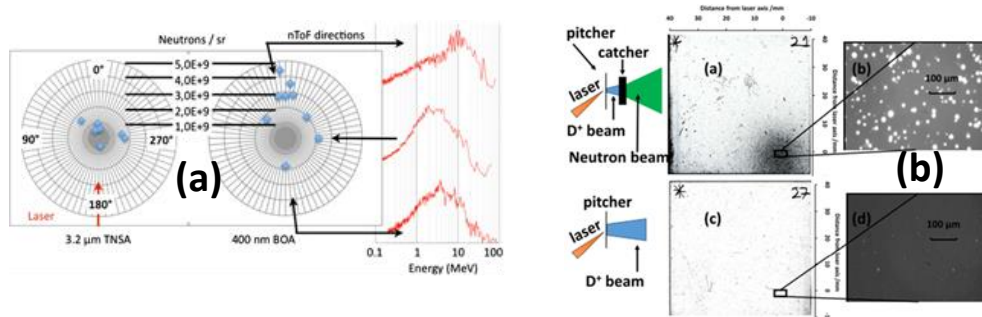
Fig. 24 – (a) and (b) shows recent experimental data showing beamed neutron emission from pitcher catcher configuration employing high energy projectile ions, (reproduced with permission from [151] and [150] respectively).

The neutron beam divergence also depends strongly on the divergence of the projectile ions – neutron beam divergence from the catcher will be a convolution of divergence of input ion beam and the neutron beam divergence expected for a collimated beam of ions. Therefore, the neutron flux on the irradiated sample can be simply improved by means of controlling divergence of the ions, provided no ions are lost during the process. The large divergence of ions produced by the TNSA mechanism present specific challenges in this regards. Using curved targets, instead of flat foil targets, has been recently shown to be highly efficient for achromatic focusing of TNSA protons [153]. The novel coil targets discussed above can also be implemented for this purpose – for example, by using a coil of conical helix shape, instead of the cylindrical helix shown in Fig. 20, one can, in principle, collect ions from larger solid angles to be guided through. Moreover, by using carefully chosen radius and pitch, one can either choose to guide a given range of ion energy or to achieve achromatic collimation by acting on the protons close to the target before they are temporally dispersed. Using a narrow energy band ion spectrum with extremely low divergence may have an additional advantage of producing a narrow energy band neutron beam [154], so that, in addition to be a better source for irradiation experiments, the neutron pulse duration will be maintained over a reasonable distance from the source.

3.3.4. Gamma and X-ray generation from laser-target interaction

A. Betatron radiation

Similarly to classical synchrotrons, X-rays can be generated by high-power lasers interacting with gas jets. This application of high intensity laser has been demonstrated [155] by focusing the laser onto a gas jet and hence the accelerated

electrons underwent betatron oscillations. The outcome was the generation of femtosecond pulsed synchrotron radiation with up to 10 keV energy. Also, the radiation was highly collimated, with a 50 mrad cone angle.

It has also been shown [156] that gamma rays can also be produced by enhancing the betatron amplitude when the electrons interact with the rear of the laser pulse. Thus, for 700 MeV accelerated electrons, gamma rays with spectra peaking between 20 and 150 keV were observed as well as high energy photons between 1 and 7 MeV.

B. X-rays generated by laser-solid target interaction

When a high power laser is focused onto a solid target, a high-temperature plasma is formed. Subsequently an ultrafast X-ray pulse is emitted when the incident laser pulse has femtosecond duration [157]. In this way, Kα sources can be obtained with energies as a function of the irradiated material (Al at 1.5 keV; Ca at 3.7 keV; Fe at 6.4 keV) [158]. This type of radiation is particularly suited to laser-based X-ray diagnostic. Recently [69] it has been shown that femtosecond lived laser pulses can be trapped in an array of metallic nanowires and X-ray M-shell spectra were observed.

C. All-optical Compton gamma-ray source

Another interesting way of producing gamma-rays by means of femtosecond laser pulses is the method based on the Compton scattering of photons by the relativistic electrons produced by laser plasma acceleration. In this way [159] gamma rays with hundreds of keV.

We envisage that in the experimental room E5, we will be able to generate X-rays by means of at least two of the above methods (A and B) for X-ray diagnostics as well as direct X-ray material irradiation.

3.4. DIAGNOSTICS

3.4.1. Electron spectrometer

For the characterization of the electron beam obtained in the gas jet, the main tool will be a dipole magnet spectrometer as shown in the figure below.

Fig. 25 – Schematic description of a 1.2 T magnetic spectrometer with an energy range 0.03-1.1 GeV (reproduced with permission from [160]).

In our configuration the electron spectrometer will be placed outside the interaction chamber as depicted in the Fig. 26.

Fig. 26 – 3D CAD design of the interaction chamber and electron spectrometer in the long focal length (F/20) configuration.

3.4.2. Thomson Parabola

The "positive-ray" parabola, nowadays called the Thomson parabola, was constructed in 1913 by J.J. Thomson in Cambridge by means of which, he discovered two isotopes of neon. The operation principle of the Thomson parabola is as follows:

charged particles entering a pinhole, pass through parallel electric and magnetic fields, and hence are deflected according to their charge to mass ratio.

A scheme of such a device used in the diagnostics of laser accelerated charged particles is shown in the figure below [161].
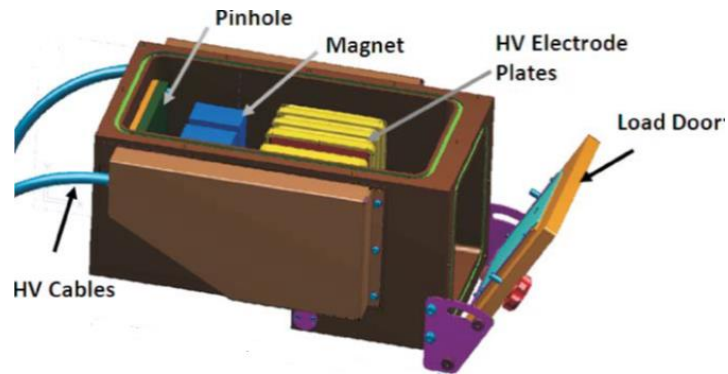

Fig. 27 – Schematic of a Thomson parabola (reproduced with permission from [161]).

In our configuration the Thomson parabola will be placed inside the interaction chamber as depicted in the figure below.
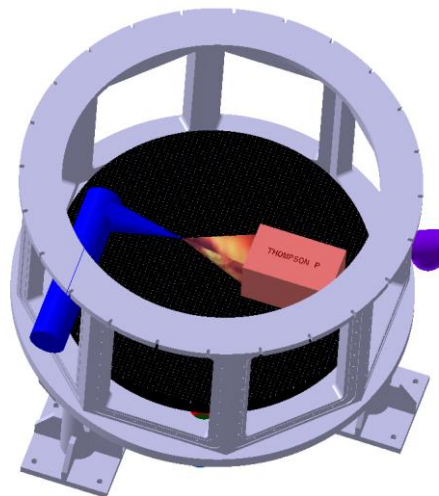

Fig. 28 – 3D CAD design of the interaction chamber in the short focal length configuration and the Thomson parabola for proton/ion diagnostic.

3.4.3. Synchronized few-cycle probe pulse set-up

If the acceleration dynamics is to be investigated experimentally, diagnostics are required which can resolve the temporal and spatial scales inherent to the acceleration process. In recent experiments, its potential to give an insight into, *e.g.*, laser-wakefield acceleration of electrons could be shown. With this technique, the laser-generated plasma wave could be visualized with unprecedented detail (see Fig. 29). Having such a diagnostic tool available will significantly enhance the experimental possibilities of this laser-facility.
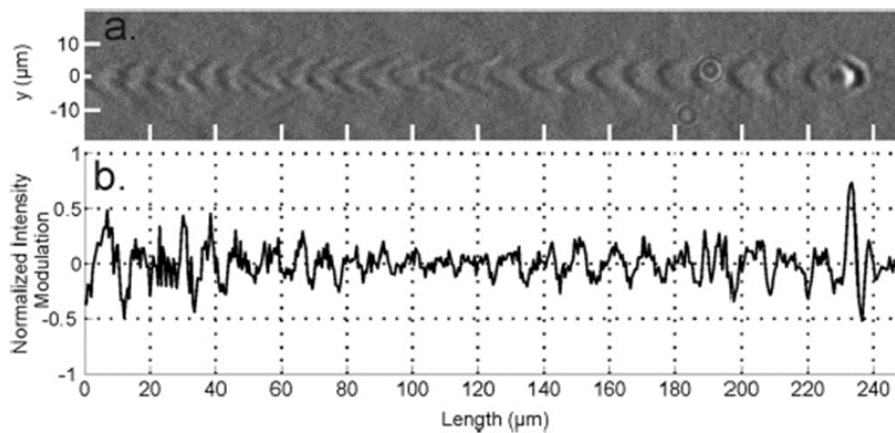

Fig. 29 – Image of a laser-driven plasma wave obtained with a few-cycle probe pulse, (reproduced with permission from [162]).

This implementation should be planned from the beginning, since space and access constraints might reduce the possibilities with this diagnostic when implemented at a later stage. To provide such a synchronized, few-cycle probe pulse for experiments, a fraction of the compressed main beam needs to be split off, sent *e.g.,* into a noble-gas filled hollow core fiber for spectral broadening and then compressed *e.g.,* by reflections off of chirped mirrors. As a result, this probe pulse can easily be shorter by a factor of 5-6 when compared to the main pulse. This allows for sub-main pulse probing of laser-plasma interactions. When used in a transverse probing configuration, the laser-generated plasma is backlighted from the side and then imaged onto a CCD camera with a high-resolution

Certain detailed aspects should be taken into account when planning the setup for this probe-pulse facility.

1. The laser energy available in the probe pulse should be high enough to provide an intense backlighter for the plasma, *i.e.* that the probe pulse can outshine self-emission from the plasma or scattering from the main laser pulse. When using a

hollow-core fiber, the energy throughput is limited to around 1 mJ for an input pulse of 30 fs. Here, the intensity and power need to lie in between the thresholds necessary to trigger the non-linear frequency conversion (which in principle works better for higher intensities in the gas) and the threshold for plasma formation (which sets an upper limit to the intensity).

2. The possibility to vary the probe beam spectrum (especially when the duration of the probe pulse is not most important) should be taken into account. For some applications, a probe frequency which is well-separated from a multiple of the fundamental laser frequency might be useful. Here, spectral broadening can help. However, also the possibility to use optical parametric amplifiers should be considered. Here, synchronized pulses with significantly higher energy and much more variable spectral shapes can be generated.

3. Since the main and probe pulse need to arrive at the interaction region at the same time, the path lengths of the two pulses need to be identical. Here, the space and length requirements for the manipulation of the probe pulse's spectrum need to be considered. One possibility is to split off a fraction of the compressed high-power pulse after the grating compressor and before it is sent towards the target area. The length consideration are important for spectral broadening in a hollow-core fiber (which usually has a length of around 1 m) including compression of the pulse before entering the fiber, focusing of the pulse into the fiber with a large F-number, the re-collimation after the fiber and the final compression. Furthermore, when using an OPA for spectral manipulation this length considerations are even more important, since the optical path lengths inside the OPA may be much longer and need to be matched by the path length of the main pulse.

3.4.4. Velocity Interferometer System for Any Reflector (VISAR)

The VISAR is a standard diagnose system for high velocity measurements. In our envisaged experiments it will be needed as a measure for the impact on solid surfaces caused by laser-driven shock waves.
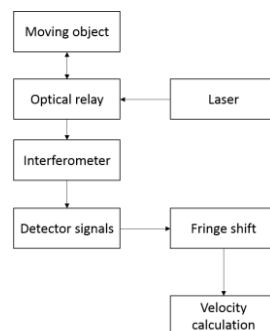

Fig. 30 – Scheme of a VISAR working principle.

3.4.5. Passive detectors

The laser driven ion or electron beams will need to be manipulated (*e.g.* energy sectioned or cleaned of other particles and radiation) as well as transported and monitored. This require single-shot beam diagnosis: ion species, spatial (divergence, size, etc.) and energy distribution. Passive detectors such as Gafchromic films, image plates, CR39 track detectors are routinely used in high intensity laser mater interaction [163, 164]. While not fully suited for extensive use at the high repetition rate of the ELI-NP lasers, they are necessary in certain experiments and for calibration and validation of online detectors as they have broader spectral sensitivity, excellent resolution and specificity.

A. Radiochromic (Gafchromic) Films

Radiochromic films, which changes its optical density when irradiated by ionization radiation (electrons, X-ray, ions, etc) are going to be used primarily in the diagnosis of the laser accelerated beam. The optical density of RCF's depend linearly to the dose delivered up to high values (1000 Gy), thus being suited for high fluxes of radiation. Radiochromic films (RCF), placed in a stack configuration and optionally sandwiched between copper or aluminium absorbing layer, are going to be used to obtain 3D image of the spatial and energy distribution of the laser accelerated ions (radio-chromic imaging spectroscopy [165]. They will be also used in conjunction with Thomson parabola or ion wide angle spectrometers to obtain the ion species composition. The mean range in these films is around 25 MeV/u). As a passive, plastic detector, is immune to electromagnetic pulse thus can be placed close (few centimeters) behind the target. RCF films batches need to be calibrated with a known ion beam flux and are post-processed at latest 24h after exposure. For post processing a CCD based document scanner can be used.

B. CR39

CR39 are plastic polymer track detector that can be used in a stack configuration for beam profiling as well as detector for Thomson parabolas or ion wide angle spectral detector. The advantage of using them is insensitivity to photons, electrons or above 10 MeV protons. Thus they are especially required when different species of ions must be characterized [125].

C. Image Plates (IP)

Image plates are 2D imagining sensors used in conjunction with Thomson parabola's and ion/electron spectrometers. Similar to RCF, image plates are sensitive to broader range of radiation kinds, have great dynamic range and sensitivity making them suited for the high radiation fluxes present in high power laser experiments [166]. The IP films contains layers of phosphorus elements that are driven in metastable excited states when excited by radiation and post-processed through optically

stimulated luminescence by a laser scanner. The spatial resolution is in the range of 25-50 mm. One advantage of IPs is that they are reusable.

3.5 EXAMPLES OF EXPERIMENTS

3.5.1. Irradiation of accelerator materials

In the case of accelerator materials irradiations, two experiments are envisaged: firstly, the sample will be irradiated with a proton beam and then the sample will be tested by two interfering shock waves as seen in the figure below.

Fig. 31 – Schematics of envisaged interfering shock waves experiments.

3.5.2. Irradiation of materials for space radiation studies

A. Degradation of optical crystals and solar cells in space

The radiation occurring in space often has exponential or power-law energy spectra, since the acceleration mechanisms produce distributions that follow statistical laws. They are not easy to reproduce in the environment of standard accelerators, which due to reliance on resonance produce nearly mono-energetic distributions. Such linear accelerators are used in present for testing the solar cells EOL efficiency [41]. At ELI-NP the highest fluence of LPA radiation in the world will be obtained. Therefore, we propose to use ELI-NP facilities for accelerated testing of the degradation of optical crystals and solar cells performance in space-like irradiation conditions

A new alternative is proposed here namely to use a laser-plasma accelerator [41] in order to emulate the space conditions for accelerated testing of the solar cells efficiency degradation. Likewise, similar defect structure and optical proprieties

modification induced by cosmic radiation in fluoride crystals can be studied in such a configuration. The effects of irradiation on the luminescence efficiency as well on the other spectral and thermal properties of the fluorides will be investigated.

Tasks:

- To measure the solar cell parameters at BOL (beginning of life).
- To study the structural defects-dislocations in $(Ba/Ca)F_2$ crystals before irradiation.
- Absorption/transmission IR-VIS-UV spectroscopy of $(Ba/Ca)F_2$ crystals before irradiation.
- To expose the solar cells and grown fluoride crystals to an electrons and protons flux generated by LPA – ELI.
- To measure the solar cell parameters at EOL (end of life).
- To study the structural defects-dislocations in $(Ba/Ca)F_2$ crystals after irradiation.
- Absorption/transmission IR-VIS-UV spectroscopy of $(Ba/Ca)F_2$ crystals after irradiation.

All electrical parameters of the solar cell should be carried out under AM0 condition.

B. **Doped fluoride crystals irradiation for fundamental studies of optical properties modification**

The irradiated induced defect structure depends on the energy of the particle radiation. The possibility to obtain a heterogeneous energy spectra of the electron and proton beams though LPA in a single laser shot is useful for making a fast, cost-effective and simultaneous exposure of different segments of a crystalline probe (or of various probes) at different energies in different positions by using a deflecting magnetic field, as proposed in [41]. A very important aspect of LPA use for radiation induced optical defects in crystals also concerns the availability of an easily tunable and cheap proton source, compared to the high costs involved with classical proton accelerators. Also, charge conversions from Yb^{3+} to Yb^{2+} could be rapidly reached with the high dose per pulse of the LPA radiation obtained at ELI-NP, for the improvement of the UV emission intensity of Yb^{2+}, which can be used in lasers for psoriasis treatment.

Tasks:

- Growth of various rare earth concentrations doped $(Ba/Ca)F_2$ crystals at WUT.
- Absorption/transmission IR-VIS-UV spectroscopy of various concentrations rare earth doped $(Ba/Ca)F2$ crystals before and after irradiation.

−   Dielectric spectra of various concentrations rare earth doped (Ba/Ca)F2 crystals before and after irradiation.

3.5.3 Technical proposal for irradiation of biological systems

Various technical aspects regarding the irradiation of biological samples are detailed below.

A. **Irradiation platforms for preclinical studies**

As a preparation of a logistic support for irradiation of bio-materials studies at ELI-NP, the facility will provide a Bio-Lab Unit for cell culture and animal tissue handling, sample conservation and measurements necessary immediately after irradiation. This unit will also offer support and preparation of experiments prior to moving the samples in the irradiation area. The Bio-Lab Unit should provide adequate conditions for long-term cell cultures, *i.e.* 37°C, controlled CO_2 and O_2 environment, and humidity, temporary handling of small animals (mice) and tissue harvesting. It is not envisioned any experimental development using pathogenic agents (viruses, bacteria, fungi) at ELI-NP.

After the primary processing of samples (normal/diseased cells or animal tissue) at ELI-NP, more processing, test-oriented will follow in the specialized laboratories at the National Institute of Pathology Victor Babes (INCDVB), located in Bucharest. Support will be provided also by relevant departments at the National Institute for Physics and Nuclear Engineering Horia Hulubei (IFIN-HH). For exposure to radiation of *in vitro* and *in vivo* samples, adequate small chambers will be designed and built to adapt 2D cell monolayers, 3D cell volumes or laboratory animals, depending on specific study requirements. For the *in vivo* studies on animal models regarding the new irradiation approach in cancer (2nd stage of the study) the irradiation platform will be connected to a performant imagistic equipment, such as mini CT or PET-CT. This is necessary for precisely locating the tumor for directing the radiation beam towards tumors, whilst sparing normal tissues. The irradiation platforms will provide both diffuse radiation, relevant for mimicking GCR-like effects, and a highly focused radiation beam, relevant for cellular irradiation and thus attenuators and collimators will be designed and built.

The use of small laboratory animals will only be limited for studies where significant understanding from *in vitro* experiments will first be achieved and will follow the European and Romanian laws and regulations. All licenses necessary will be obtained from the appropriate regulatory agency ANSVSA ("Autoritatea Nationala Sanitar-Veterinara si pentru Siguranta Alimentelor"- National Agency for Animal Welfare and Food Safety). In addition an ethical committee for welfare of

animals used in experiments similar to those acting in universities and the affiliated research institutes from other European countries (*i.e.* UK, France, Belgium), will be based in the Department of Life and Environmental Sciences at National Institute of Physics and Nuclear Engineering (IFIN-HH) and will approve the experimental protocols that will guarantee the welfare of animals during experiments.

The new development at ELI-NP facility will be from *in vitro* investigations to animal studies, from "rough" effects to molecular mechanisms of action, from multi-parameter screening using "omics" technologies to validation of particular biomarkers and mechanisms. Due to the absolute novelty of the ELI-generated ionizing radiation, such a comprehensive approach is mandatory. Previous results obtained using less complex irradiation models will only guide this study. Many physiologic processes should be tackled for generating a realistic biologic image of the multi-component radiation effects on complex organisms.

B. General Protocols

a. Biological samples
    –   2D and 3D cultures of normal, cancer and inflammatory cells (primary cells and cell lines) will be used.
    –   Normal and transgenic small laboratory animals (animal models for various pathological conditions), will be purchased from The Jackson Laboratory, USA, and will be further maintained in standardized conditions at the animal care facility of INCDVB and IFIN-HH.
    –   Tissues/cells harvested from the irradiated animals, preserved for various biomedical tests, will be stored until use in the deep freezing unit of INCDVB, using standardized bio-banking procedures.

b. Biomedical investigations
    –   *In vitro* cellular studies
        –   phenotyping (immunochemistry, confocal microscopy, flow cytometry), viability tests, taking into account a panel of cellular death types (confocal microscopy, flow cytometry)
        –   cell proliferation (flow cytometry, impedance measurements on adherent cells)
        –   genotoxicity (micronuclei test on bone marrow cells)
        –   oxidative stress and the antioxidant response (flow cytometry, pathway-focused PCR array, signal reporter assay)
        –   cellular secretory activity (ELISA, protein multiplexing by Luminex or protein microarray)
        –   signal transduction pathways (Western blot, intracellular protein multiplexing using Luminex)
        –   genetic instability assessed by karyotyping

- gene expression profile (PCR array, gene microarray)
- epigenomic investigation (total and specific methylation status, chromatin immuno-precipitation, micro RNA profile)
- *In vivo* studies in animal models
  - *in vivo* imaging of animals (IFIN-HH)
  - (ultra)structural *ex vivo* investigation of cells/tissues (high resolution transmission electron microscopy, histological and immuno-histochemical investigation)
  - organ toxicity and signal transduction events (gene expression by pathway-focused PCR arrays, gene microarray) and further validation of candidate genes by RT-PCR
  - classical cytogenetic investigation (karyotyping) for assessing genetic instability
  - epigenomic investigation (microRNAs profile in cells/tissues/serum)
  - protein profiling in serum (Luminex, protein microarray, SELDI-TOF mass spectrometry) and further validation of protein biomarkers by ELISA/Western blot
  - immunologic screening: immuno-phenotype, functional investigation of the adaptive and innate immune response (T lymphocytes and macrophages polarization, the cytokine profile, oxidative stress and the antioxidant response).

A flow chart describing the experimental steps and data management is shown in Fig. 32.

A specific study is detailed below:

Non-targeted effects induced by low dose "mix" of secondary radiation beams accessible at ELI-NP. Bystander and adaptive responses to space like radiation exposures.

The project is based on the irradiation capabilities offered by ELI-NP facility: a complex tunable, multicomponent and multienergetic radiation which will mimic Cosmic ray stressful conditions. For the near future the most important problem to address in this domain is the radiation risk estimation for the solar system travels.
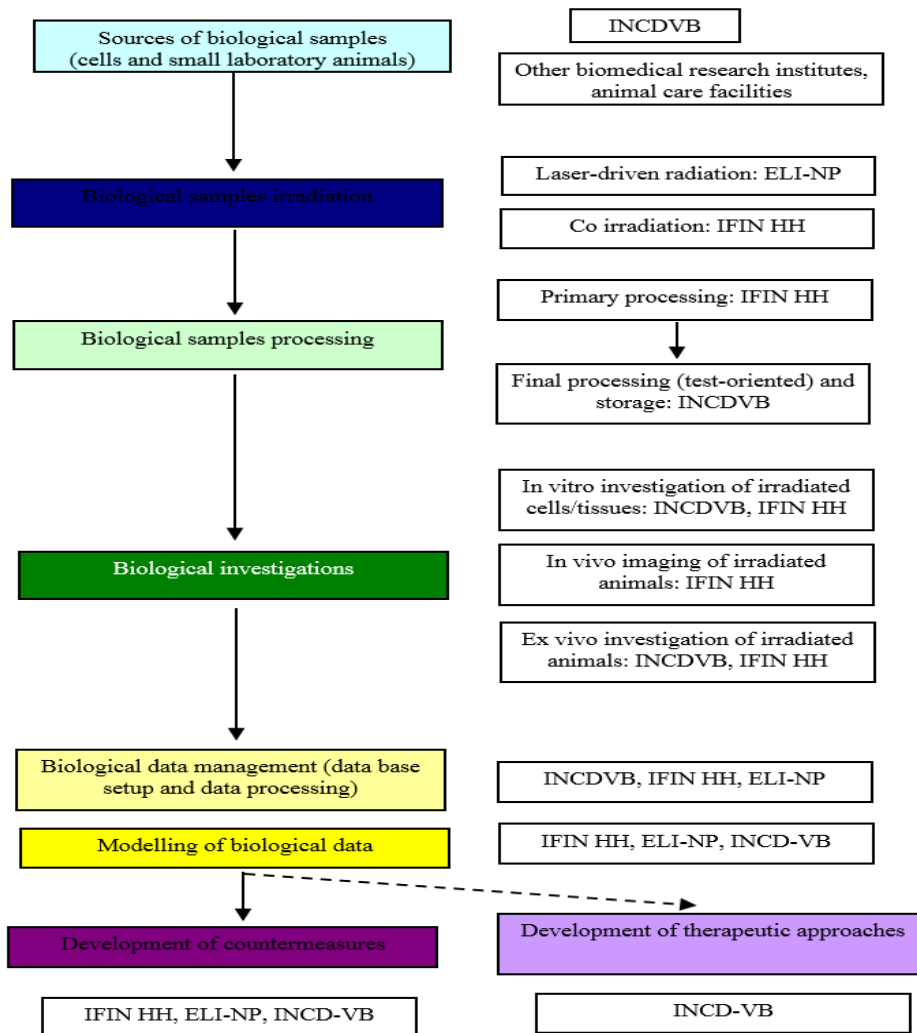
Fig. 32 – Flowchart of activities for envisaged biological research at ELI-NP.

The lack of detailed knowledge of the biological effects of energetic heavy ions especially at low dose and low dose rates (low fluences) constitutes the major source of uncertainty for risk estimates [167, 74]. The exposure risks for astronauts to solar system irradiation has 2 components [168, 169]:

- Acute risks can be associated to solar energetic particle events (SEP) (up to 900 mSv).

- Late stochastic risks associated to the chronic exposure to galactic cosmic rays (GCR) providing doses up to 100-fold Earth's background (approximately 100-300 mSv/year).

The predominance of protons for each of the sources of space radiation was demonstrated and dose measurements have been performed during space missions. The conditions estimated to be offered by ELI-NP for proton irradiation mimics the lowest part of the galactic radiation component in terms of particle energy (around 20 MeV) and the solar flare radiation in terms of fluency (more than 10^{10} particles/pulse).

The radiobiology literature outlines some specific research issues separately for acute effects or for late stochastic effects [170, 171, 35].

Main research issues for acute effects: (i) how is the RBE of protons or heavier ions modified at low dose rate (low fluency); (ii) how is the radiosensitivity of individuals modified by the space environment, *i.e.* microgravity conditions or hipergravity; (iii) what are the most effective biomedical countermeasures for acute effects as long as the present radioprotective drugs are toxic and the antioxidants not effective.

Main research issues for late stochastic effects point to cancer risk, central nervous system (CNS) risk or to cardiovascular risk. Damage at low fluencies induced by heavy ions may be both quantitatively and qualitatively different from low dose low LET exposures. In vitro acceleration studies are needed at DNA, chromosomal, tissue and gene expression level to assess the relevance of the different types of damage and different potential processing. Furthermore, multiple stressors in the cosmic environment can lead to synergistic or antagonistic effects. Regarding the CNS risk, accelerator experiments using innovative model systems are needed, *e.g.* human tissues. It is also important to conclude if there is or not a threshold for late non-cancer irradiation effects.

It is important to keep in mind that exposures in CR environment occur at low fluencies and fluency rates, meaning that particle traversals through cells in the body are well separated as tissue location and time. Non-targeted effects as bystander response may have increased significance [172]. Our research proposal intend to address some of the problems not-understood yet in the low dose radiobiology domain which concern also space radiation exposures - like bystander responses, hyper radiation sensitivity, adaptive or synergic response to repetitive low dose exposure or to alternation of repetitive low dose and acute high dose of energetic protons or heavy ions. The group will take advantage of our previous experience in the low dose and bystander effects of irradiation [173–177].

Proposed irradiation protocols:
- Separate irradiations: proton single dose irradiation (dose domain 0-5 Gy); electron single irradiation (dose domain 0-5 Gy); and reference X ray or gama irradiation (dose domain 0-5 Gy).
- Repetitive irradiations – sequences of exposures of lower doses (0.1-0.5 Gy), up to total doses of 5 Gy.
- Alternative irradiations in the experiments of bystander and adaptive responses: low dose irradiations (less than 0.5Gy) followed by repetitive or single irradiations of doses up to 2-5 Gy.
- The alternative irradiation protocols will combine exposures to different beam types (protons, electrons, gamma, brilliant X-ray).
- The irradiation regimes will include repetitive low fluence exposures, single short high fluence exposures or combination of them.

Biological models and end-points:
The experiments will be performed on human and rodent cell lines, especially fibroblasts and brain cells. Normal human cell lines expressing fluorescent markers will be preferred, as being the most promising biological systems for preliminary radiobiology experiments on CR. Genetically engineered cell lines to constitutively express fluorescent markers (such as green-fluorescent proteins or luciferase) will allow to monitor transcriptional activity of specific promoters, thus providing real time information on the viability and metabolic activity of the cells. In addition this biological model will allow live visualization (by fluorescent microscopy) of recruitment of DNA repair proteins to sites of particle hits and the temporal evolution of such damage tracks. Bioluminescence assays will be applied to monitor metabolic pathways activated in response to radiation and stress or other end-points expected to be altered in reduced microgravity, such as cytoskeleton functional status [178]. In parallel, we intend to develop a 3-dimensional tissue model in order to study mechanisms and importance of bystander responses in the used regime of irradiation.

The investigated end-points in the experiments about DNA toxicity and repair, cellular toxicity and genomic instability will be: MN induction (light and fluorescent microscopy), H2AX expression (using fluorescent image analysis), other DNA repair pathways (using western blotting, PCR), clonogenic cell survival (microscopy assays), apoptosis induction and mitochondrial transmembranal potential (using fluorescent image analysis). The bystander experiments will be performed predominantly in co-culture arrangements.

Irradiation experiments of biological samples with multi-component, multi-energetic beams require development of several experimental setups depending on the specifics goal of the study and the type of bio-sample. Cell monolayers are usually grown inside a standard 96 well plate ($127.7 \times 85.48 \times 14.6$ mm^3). The plate can be sealed with polyethylene sealing film. The 96 well plates are made of hard plastic (polystyrene). The advantage of irradiating a large number of samples simultaneously is the relevant statistics, a requirement in the experimental studies in-vitro. In addition a 96 well plate is accommodated by most assay equipment for post processing and measurements.

SRIM-TRIM simulations were used for set-up design and optimization. For irradiation of the 96 well plate inside the interaction chamber a cassette will be built to protect the samples from vacuum environment but still allowing the irradiation through the Al or Ni window. This cassette will be filled with air at atmospheric pressure and the content will be maintained at 37°C.
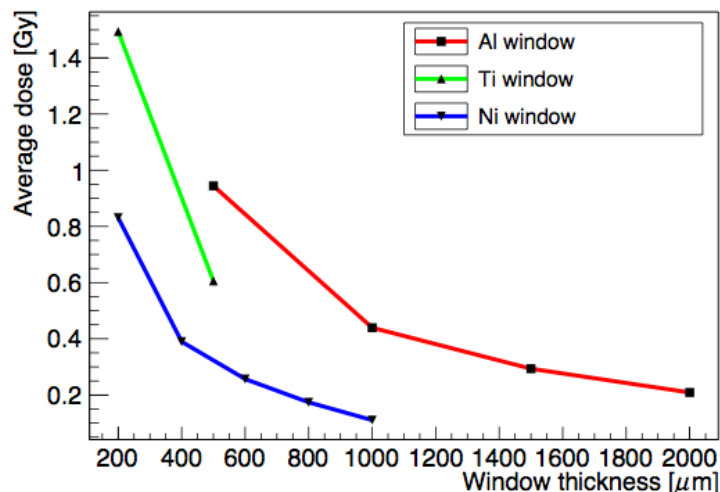

Fig. 33 – Average dose deposited in a cell monolayer as a function of window thickness (preliminary results from Geant4 simulations of the irradiation setup).

Geant4 simulations have shown that depending on the thickness of the window and the material used doses ranging from 0.1 to 1.5 Gy can be applied to the cell monolayer as seen in Fig. 33. The target insertion system can be used to manipulate the cassette containing the samples. Suspensions of cell, organoids or tissue will require variations of the experimental setup to ensure uniform irradiation.

4. CONCLUSIONS

This paper described the future experiments that will take place in the E5 experimental area of ELI-NP. This particular station within the facility will host two arms of the high power laser system, namely two 1 PW lasers with a repetition rate of 1 Hz. This capability will enable researchers to perform various experiments with high power lasers as well as secondary sources generated by these lasers, in the fields of materials science as well as biological physics.

REFERENCES

1. H. Geissel *et al.,* Technical Report on the Design, Construction, Commissioning and Operation of the Super-FRS of FAIR, GSI Report 2005-02, (2005).
2. N. A. Tahir, A. Kozyreva, P. Spiller, D. H. H. Hoffmann, and A. Shutov, Phys. Rev. E **63**, 036407 (2001).
3. G. Heidenreich, AIP Conf. Proc. **642**,122-124 (2002).
4. H. Geissel, H. Weick, M. Winkler, G. Münzenberg, V. Chichkine, M. Yavor, T. Aumann, K. H.Behr, M. Böhmer, and A. Brünle, Nucl. Instrum. Methods Phys. Res. B **204**, 71-85 (2003).
5. R. Bernath, C. G. Brown, J. Aspiotis, M. Fisher, M. Richardson, Proc. SPIE **6219**, 62109A (2006).
6. P.K.F. Grieder, *Cosmic Rays at Earth* (Elsevier, Amsterdam, 2001).
7. R. A. Mewaldt, Adv. Space Res. **14**, 737-747 (1994).
8. K. Yoshida, Adv. Space Res. **42**, 477–485 (2008).
9. M Kim, J Wilson, and F Cucinotta, Adv. Space Res. **37**, 1741-1748 (2006).
10. R. Battiston, P. Blasi, M.T. Brunetti, D. De Marco, P. Lipari, B. Sacco, and A. Santangelo*,* Adv. Space Res. **37**, 1834–1840 (2006).
11. R. Nymmik*,* Adv. Space Res. **38**, 1182–1190 (2006).
12. J. L. Barth, C. S. Dyer, and E. G. Stassinopoulos, IEEE Transactions on nuclear science **50**, 446-482 (2003).
13. G Reitz, Z. Med. Phys. **18**, 233–243 (2008).
14. M.V. Podzolko, I.V. Getselev, Y.I. Gubar, I.S. Veselovsky, and A.A. Sukhanov, Adv. Space Res. **48**, 651–660 (2011).
15. V. Benghin, V. Petrov, S. Kireeva, A. Markov, A. Volkov, A. Aleksandrin, M. Panasjuk, J. Kutuzov, O. Morozov, and M. Teltsov, Adv. Space Res. **36**, 1749–1752 (2005).
16. R. Mewaldt, A. Davis, W. Binns, G. Nolfo, J. George, M. Israel, R. Leske, E. Stone, M. Wiedenbeck, and T. Rosenvinge, *29th International Cosmic Ray Conference*, 101-104 (2005).
17. O. Zeynali, D. Masti, M. Nezafat, and A. Mallahzadeh, J. Mod. Phys. **2**, 1567-1573 (2011).
18. S. Rathod, A. Saxena, and S. Dasgupta, IETE Tech. Rev. **28**, 451-469 (2011).
19. C. Liu, X. Li, H. Geng, E. Rui, L. Guo, J. Yang, and L. Xiao, Nucl. Instrum. Meth. A **677**, 61–66 (2012).

20. L. Ming, W. Rong, L. Hong, H. Tao, F. Zhao, and H. Lei, Nucl. Instrum. Meth. B **269**, 1884–1886 (2011).

21. V. Goiffon, P. Magnan, O. Saint-Pé, F. Bernard, and G. Rolland, Nucl. Instrum. Meth. A **610**, 225–229 (2009).

22. G. Hubert, S. Bourdarie, L. Artola, S. Duzellier, and J. Roussel, Acta Astronaut., **69**, 526–536 (2011).

23. J. Alvarado, E. Boufouss, V. Kilchytska, and D. Flandre, Microelectron. Reliab. **50**, 1852–1856 (2010).

24. D. Fixsen, Astrophys. J. **707**, 916–920 (2009).

25. V. Ramachandran, M. Gadlage, J. Ahlbin, B. Narasimham, M. Alles, R. A. Reed, B. Bhuva, L. Massengill, J. Black, and C. N. Foster, Solid State Electron. **54**, 1052–1059 (2010).

26. K. Miyoshi, *NASA/TM-2007-214668* (2007).

27. D. Doyle, W. Reynolds, and B. Arritt, *ASME 2010 SMASIS* (2010).

28. Orbital Debris Surface Examinations, NASA Orbital Debris Program office, (http://orbitaldebris.jsc.nasa.gov/measure/surfaceexam.html).

29. C. Hellweg, M. Thelen, A. Arenz, and C. Baumstark-Khan, Adv. Space Res. **39**, 1011–1018 (2007).

30. K. Georgea, J. Rhone, A. Beitman, and F.A. Cucinotta, Mutation Research **756**, 165– 169 (2013).

31. Z. Koliskova, L. Sihver, I. Ambrozova, T. Sato, F. Spurny, and V. Shurshakov, Adv. Space Res. **49**, 230–236 (2012).

32. P. Brekke, NATO Science Series **176**, (2003).

33. R. Maurer, M. Fraeman, M. Martin, and D. Roth, Technical Digest **28**, 17-28 (2008).

34. J. Schwank, M. Shnmeyfelt, and P. Dodd, *Sandia National Laboratories SAND-2008-6851P* (2008).

35. M. Durante, G. Kraft, P. O'Neill, G. Reitz, L. Sabatier, and U. Schneider, Adv. Space Res. **39**, 1082–1086 (2007).

36. L. Sihver, Acta Astronautica **63**, 886–898 (2008).

37. L. Sihver, Z. Med. Phys. **18**, 253–264 (2008).

38. B. Tseng, M. Lan, K. Tran, M. Acharya, E. Giedzinski, and C. Limoli, Redox Biology **1**, 153–162 (2013).

39. E. Blakely and P. Chang, Advances in Space Research **40**, 461–469 (2007).

40. M. Durante and A. Kronenberg, Adv. Space Res. **35**, 180–184 (2005).

41. B. Hidding, T. Köigstein, O. Willi, J. B. Rosenzweig, K. Nakajima, and G. Pretzler, Nuclear Instruments and Methods in Physics Research A **636**, 31–40 (2011).

42. I. Nicoara *et al.,* J. Cryst. Growth **310**, 1470 (2008).

43. M. Stef, I. Nicoara, and F. Stef, European Physical Journal B **86**, 152 (2013).

44. B. Van Gorp, P. Mouroulis, D. Blaney, R. O. Green, B. L. Ehlmann, and J. I. Rodriguez, J. Appl. Remote Sens. **8**, 084988 (2014).

45. J. Ge, A. S. Kutyrev, B. H. Dean, H. S. Moseley, B. E. Woodgate, and C. Marx, Proc. SPIE **4850**, 535 (2003).

46. H.B. Newman, in *Heavy Scintillators for Scientific Industrial Applications,* edited by F. De. Notaristefani, P. Lecoq, and M. Schneegans (Editions Frontieres, Gif-sur-Yvette, 1993), p. 5.

47. R. Zhu, *Lauritsen Laboratory, California Institute of Technology, Pasadena, USA*, (1993).

48. H.L. Cotal, D.C. Law, N.H. Karam, and S.M. Bedair, in *Physics of Nanostructured Solar Cells*, edited by V. Badescu and M. Paulescu (Nova Science, New York, 2010) pp. 251-270.

49. F. Dimroth, World Record Solar Cell with 44.7% Efficiency. *Fraunhofer ISE, Press Release* **22/13** (2013).

50. N.S. Fatermi, H.E. Pollard, H.Q. Huo, and P.R. Sharps, Proc. 28th IEEE PVSC September (2000).

51. S.R. Messenger, G.P. Summers, E.A. Burke, R.J. Walters, and M.A. Xapsos, Progress in Photovoltaics: Research and Applications **9**, 103-121 (2001).

52. S. Majewski and D. Anderson, Nucl. Instr. and Meth. A **241**, 76 (1985).

53. V. Mysore, Indian J. Dermatol. Venereol. Leprol. **75**, 119 (2009).

54. T. Mudigonda *et al.,* J. Am. Acad. Dermatol. **66**, 664 (2011).

55. J. M. Carrrascosa *et al.,* Actas Dermosifiliogr. **103**, 175 (2011).

56. J. Rubio, J. Phys. Chem. Solids **52**, 101 (1991).

57. I. Nicoara, L. Lighezan, M. Enculescu, and I. Enculescu, J. Cryst. Growth **310**, 2026 (2007).

58. V. Petit, P. Camy, J.L. Doualan, and R. Moncorgé, Appl. Phys. Lett. **88,** 051111 (2006).

59. J. L. Doualan *et al.,* Laser Physics **20**, 533 (2010).

60. S.M. Kaczmarek *et al.*, J. Phys. Condens. Matter **17**, 3771–3786 (2005).

61. W.J. Scouler and A. Smakula, Phys Rev **120,** 1154-1161 (1960).

62. S. Abuazoum, S. M. Wiggins, R. C. Issac, G. H. Welsh, G. Vieux, M. Ganciu, and D. A. Jaroszynski, Rev. Scient. Instrum. **82**, 063505 (2011).

63. M. Sozet, J. Néauport, E. Lavastre, N. Roquin, L. Gallaisband, and L. Lamaignère, Proc. of SPIE **9513***,* 951316 (2015).

64. J. Z. P. Skolski, G. R. B. E. Römer, J. Vincenc Obona, and A. J. Huis in 't Veld, Journal of Applied Physics **115**, 103102 (2014).

65. N. Šiaulys, L. Gallais, and A. Melninkaitis, Optics Letters **39***,* 2164 (2014).

66. G.S. Lodha, K. Yamashita, H. Kunieda, Y. Tawara, J. Yu, Y. Namba, and J.M. Bennett, Applied Optics **37,** 5239 (1998).

67. D. Stutman and M. Finkenthal, Rev Sci Instrum. **82***,* 113508 (2011).

68. S. Corde, K. Ta Phuoc, G. Lambert, R. Fitour, V. Malka and A. Rousse, Rev. Mod. Phys. **85** (2013).

69. M. A. Purvis, V. N. Shlyaptsev, R. Hollinger, C. Bargsten, A. Pukhov, A. Prieto, Y. Wang, B. M. Luther, L. Yin, S. Wang, and J. J. Rocca, Nature Photonics **7,** 796 (2013).

70. C.P. Lungu, Giga and tera-watt laser interaction with carbon, tungsten and beryllium films, *Internal report.*

71. C.P. Lungu, C.M. Ticos, C. Porosnicu, I. Jepu, M. Lungu, A. Marcu, C. Luculescu, G. Cojocaru, D. Ursescu, R. Banici, and G.R. Ungureanu, Applied Physics Letters **104**, 101604 (2014).

72. Ad Hoc Committee on the Solar System Radiation Environment and NASA's Vision for Space Exploration. Space Radiation Hazards and the Vision for Space Exploration. Washington DC: The National Academies Press, 7–37 (2006).

73. A. Kronenberg, and F.A. Cucinotta*,* Health. Phys. **103**, 556-567 (2012).

74. M. Maalouf, M. Durante, and N. Foray, J. Radiat. Res. **52**, 126–146 (2011).

75. MELODI: Multidisciplinary European Low Dose Initiative 2010 (http://www.melodi-online.eu/m_docs.html).

76. MELODI Statement, 15 April 2013.

77. W. Hur *et al.,* Chemistry & Biology **17**, 537–547 (2010).

78. E.N. Parker, Shielding Space Travelers, Scientific American, 40–47 (2006).

79. M. Kreuzer *et al.*, Strategic Research Agenda of the Multidisciplinary European Low Dose Initiative (MELODI), 13 June 2014.

80. A.J. Lomax, Cancer J. **15**, 285-291 (2009).

81. A. Brown and H. Suit, Radiother. Oncol. **73**, 265-268 (2004).

82. X. Yan, U Titt, and A.M. Koehler, Nucl. Instr. Meth. Phys. Res. A **476**, 429-434 (2002)

83. E.E. Klein, in *Perez and Brady's Principles and Practice of Radiation Oncology*, edited by E. C. Halperin, C. A. Perez, and L. W. Brady (Lippincott Williams & Wilkins, Philadelphia 2008), p. 190.

84. R.L. Foote *et al.,* Radiation Oncology **7,**174 (2012).

85. D. Schardt *et al.*, Rev. Mod. Phys. **82**, 383 (2010).

86. C.D. Schlaff *et al.*, Radiation Oncology **9**, 88 (2014).

87. S.H. Sahlberg *et al.*, PLOS One **9**, e94621 (2014).

88. C. Prontz, Cancer **118**, 3225 (2012).

89. J. Bensimon *et al.,* Oncogene **32**, 251-258 (2013).

90. K. Ogawa *et al.*, Anticancer Res. **33**, 747-54 (2013).

91. M. Veldwijk *et al.,* PLOS One **9**, e84991 (2014).

92. I. Sologuren *et al*., Transl. Cancer Res. **3**, 18-31 (2014).

93. H.B. Stone *et al*., Lancet Oncol. **4**, 529-536 (2003).
94. A. Marusyk and K. Polyak, Biochim. Biophys. Acta **1805**, 105 (2010).
95. M. Levi *et al.,* J. Phys. Chem. C **117**, 15369–15374 (2013).
96. H.C. Huang *et al*., Nano LIFE **1**, 289 (2010).
97. D. Katz *et al.,* Int. J. Radiation Oncology **73**, 988–996 (2009).
98. I. Miladi *et al.*, Small **10**, 1116–1124 (2014).
99. S. Viaud *et al.,* Cancer Res. **74**, 4217 (2014).
100. A.Z. Wang *et al.,* Annual Review of Medicine **63**, 185-198 (2012).
101. Z. Fan *et al.,* J. Food Drug Analysis **22**, (2014).
102. D. Henderson *et al.,* Biotechnology Journal **9**, 1104–1114 (2014).
103. T. Westdorp *et al.,* Front Immunol **10**,00191 (2014).
104. M. Vidal *et al.,* Clin. Proteomics **9**, 6 (2012).
105. J.J. McCarthy, H.L. McLeod, and G.S. Ginsburg, Sci. Transl. Med. **5**, 189 (2013).
106. R. Baskar, Genome Integrity **1**, 13 (2013).
107. P.C. Lara *et al.,* Cancer Lett. **13**, 00659-9 (2013).
108. T. Finkel, J.Chem. Biol. **194**, 7-15 (2011).
109. H. Hulsmans and P. Holvoet, J. Cell. Mol. Med. **14**, 70-78 (2010).
110. J.T. McDonald, Cancer Res. **70**, 1–10 (2013).
111. B. Aurand *et al.*, Optics Express **19**, 17151 (2011).
112. S. Keppler, M. Hornung, R. Bodefeld, M. Kahle, J. Hein, and M. C. Kaluza, Optics Express **20**, 20742 (2012).
113. I.J. Kim, I.W. Choi, S.K. Lee, K.A. Janulewicz,·J.H. Sung, T.J. Yu, H.T. Kim, H. Yun, T.M. Jeong,·and J. Lee, Applied Physics B **104,** 81-86 (2011).
114. T. Tajima and J.M. Dawson*,* Phys. Rev. Lett. **43**, 267 (1979).
115. A. Modena, Z. Najmudln, A. E. Dangor, C. E. Clayton, K. A. Marsh, C. Joshi, V. Malka, C. B. Darrow, C. Danson, D. Neely and F. N. Walsh, Nature **337,** 606 (1995).
116. D. Umstadter, S.-Y. Chen, A. Maksimchuk, G. Mourou, and R. Wagner, Science **273**, 472-475 (1996).
117. S. P. D. Mangles, C. D. Murphy, Z. Najmudin, A. G. R Thomas, J. L.Collier, A.E. Dangor, P. S. Foster, J. L. Collier, E. J. Divall, J. G. .Gallacher, C. J. Hooker, D. A. Jaroszynski, A. J. Langley, W. B. Mori, P. A. Norreys, F. S. Tsung, R. Viskup, B. R. Walton and K. Krushelnick, Nature **431**, 535 (2004).
118. J. Faure, Y. Glinec, A. Pukhov, S. Kiselev, S. Gordienko, E. Lefebvre,J.-P. Rousseau, F. Burgy and V. Malka, Nature **431**,541 (2004).
119. C. G. R. Geddes, Cs. Toth, J. van Tilborg, E. Esarey, C. B. Schroeder, D.Bruhwiler, C. Nieter, J. Cary, and W. P. Leemans, Nature **431,** 538 (2004).
120. W. P. Leemans, B. Nagler, A. J. Gonsalves, Cs. Tóth, K. Nakamura, C. G. R. Geddes, E. Esarey, C. B. Schroeder and S. M. Hooker, Nature Physics **2,** 696 (2006).
121. X. Wang, R. Zgadzaj, N. Fazel, Z. Li, S. A. Yi, X. Zhang, W. Henderson, Y.-Y. Chang, R. Korzekwa, H.-E. Tsai, C.-H. Pai, H. Quevedo, G. Dyer, E. Gaul, M. Martinez, A. C. Bernstein, T. Borger, M. Spinks, M. Donovan, V. Khudik, G. Shvets, T. Ditmire and M. C. Downer, Nature Communications **4,** 1988 (2013).
122. I. J. Kim *et. al.*, Phys. Rev. Lett. **111**, 165003 (2013).
123. A. Macchi *et. al*., Rev. Mod. Physics **85**, 751 (2013)
124. S. Kar *et al.,* Phys. Rev. Lett. **109**, 185006 (2012).
125. D. Jung *et al.,* New Journal of Physics **15**, 123035 (2013).
126. H. T. Kim, K. H. Pae, H. J. Cha, I. J. Kim, T. J. Yu, J. H. Sung, S. K. Lee, T. M. Jeong and J. Lee, Phys. Rev. Lett. **111**, 165002 (2013).
127. J. Green *et al.,* Appl. Phys. Lett. **104**, 214101 (2014).
128. J. Fuchs *et al.,* Nat. Phys. **2**, 48 (2006).
129. M. Borghesi *et al.,* Appl. Phys. Lett. **82,** 1529 (2003).
130. S. Kar *et al.,* High Energy Density Phys. **4**, 26 (2008).

131. S. Kar *et al.,* Phys. Rev. Lett. **100**, 105004 (2008).
132. S.C. Wilks *et al.,* Phys. Rev. Lett. **69**, 1383 (1992).
133. L. Disdier *et al.,* Phys. Rev. Lett. **82**, 1454 (1999).
134. H. Habara *et al*., Phys. Rev. E **70**, 046414 (2004).
135. H. Habara *et al.,* Phys. Rev. E **69**, 036407 (2004).
136. D. Hilscher *et al.,* Phys. Rev. E **64**, 016414 (2001).
137. N. Izumi *et al.,* Phys. Rev. E **65,** 036413 (2002).
138. G. Pretzler *et al.,* Phys. Rev. E **58**, 1165 (1998).
139. A. Kodama *et al.,* Plasma Phys. Controlled Fusion **41,** A419 (1999).
140. A. Youssef *et al.,* Nucl. Fusion **50**, 035010 (2010).
141. V.S. Belyaev *et al.*, Laser Phys. **16,** 1647 (2006).
142. V.S. Belyaev *et al.*, Journal of Experimental and Theoretical Physics **98**, 1133 (2004).
143. L. Williangle *et al.*, Phys. Plasmas **18**, 083106 (2011).
144. P. Norreys *et al.*, Plasma Phys. Controlled Fusion **40,** 175 (1998).
145. C. Zulick *et al.,* Applied Physics Letters **102,** 124101 (2013).
146. G.M. Petrov *et al.,* Phys. Plasmas **19**, 093106 (2012).
147. D.P. Higginson *et al.,* Phys. Plasma **18,** 100703 (2011).
148. D. P. Higginson *et al.,* Phys. Plasma **17**, 100701 (2010).
149. K.L. Lancaster *et al.,* Phys. Plasma **11**, 3404 (2004).
150. S. Kar *et al.,* arXiv:1507.04511.
151. M. Roth *et al.,* Phys. Rev. Lett. **110**, 044802 (2013).
152. J. Davis and G.M. Petrov*,* Plasma Phys. Control. Fusion **50**, 065016 (2008).
153. S. Kar *et al.,* Phys. Rev. Lett. **106**, 225003 (2011).
154. C. A. Ellison and J. Fuchs, Phys. Plasmas **17**, 113105 (2010).
155. A. Rousse, K.T. Phuoc, R. Shah, A. Pukhov, E. Lefebvre, V. Malka, S. Kiselev, F. Burgy, J. Rousseau, D. Umstadter, and D. Hulin, Phys. Rev. Lett. **93**, 135005 (2004).
156. S. Cipiccia *et al.*, Nature Physics **7**, 867-871 (2011).
157. M. M. Murnane, H. C. Kapteyn, M. D. Rosen, and R. W. Falcone, Science **251,** 531 (1991).
158. A. Rousse, P. Audebert, J. P. Geindre, F. Fallies, J. C. Gauthier, A. Mysyrowicz, G. Grillon, and A. Antonetti, Phys. Rev. E **50**, 2200 (1994).
159. K. Ta Phuoc, S. Corde, C. Thaury, V. Malka, A. Tafzi, J. P. Goddet, R. C. Shah, S. Sebban, and A. Rousse, Nature Photonics **6**, 308 (2012).
160. K. Nakamura, B. Nagler, Cs. Tóth, C. G. R. Geddes, C. B. Schroeder, E. Esarey, and W. P. Leemans, A. J. Gonsalves and S. M. Hooker, Physics of Plasmas **14**, 056708 (2007).
161. C. G. Freeman, G. Fiksel, C. Stoeckl, N. Sinenian, M. J. Canfield, G. B. Graeper, A. T. Lombardo, C. R. Stillman, S. J. Padalino, C. Mileham, T. C. Sangster, J. A. Frenje, Review of Scientific Instruments **82,** 073301 (2011).
162. M. B. Schwab, A. Saevert, O. Jaeckel, J. Polz, M. Schnell, T. Rinck, L. Veisz, M. Moeller, P. Hansinger, G. G. Paulus, and M. C. Kaluza, Applied Physics Letters **103,** 191118 (2013).
163. P. Bolton *et al.,* Physica Medica **30**, 255 (2014).
164. M. Roth, Journal of Instrumentation **6**, R09001 (2011).
165. F. Nuernberg *et al.*, Review of Scientific Instruments **80**, 033301 (2009).
166. I.J. Paterson, R.J. Clarke, N.C. Woolsey, and G. Gregori, Measurement Science and Technology **19**, 095301 (2008).
167. K. Held, Int. J. Radiat. Biol. **85**, 379-390 (2009).
168. J.H. Adams *et al*., Advances in Space Research **40**, 338–341 (2007).
169. M. Durante, Planetary and Space Science **74**, 72-77 (2012).
170. ESA-IBER Preparatory Study of Investigations into Biological Effects of Radiation—Final Report ESA-CR(P) **4585** (2006).
171. NASA. Bioastronautics Roadmap. NASA SLSD (2008).
172. J. Domogauer and E.I. Azzam, Bystander effects and space radiation, *NASA Summer School 2013* (2014).

173. D.I.Savu, N. Moisoi, and I. M. Petcu, Journal of Radioanalytical and Nuclear Chemistry **253**, 21-23 (2002).
174. I. Petcu, D. Savu, H. Thierens, G. Nagels, and A. Vral, International Journal of Radiation Biology **82**, 793-803 (2006).
175. D. Savu, I. Petcu, M. Temelie, C. Mustaciosu, and N. Moisoi, Mutation Research – Fundamental and Molecular Mechanisms of Mutagenesis **771**, 13–20 (2015).
176. I. Petcu, D. Savu, A. Vral, H. Thierens, Guy Nagels, and L. De Ridder, International Journal of Radiation Biology **80,** 663-672 (2004).
177. M. Bacalu, B. Zorila, and M. Radu, Analyt. Biochem. **440,** 123–129 (2013).
178. E.L. Kordyum *et al.*, Acta astronautica **56**, 613-621 (2005).